SOURCE PARAMETERS AND STRESS RELEASE OF SEISMIC SEQUENCES OCCURRED IN THE FRIULI-VENEZIA GIULIA REGION (NORTHEASTERN ITALY) AND IN WESTERN SLOVENIA

Gianni Bressan[1], Stefano Kravanja[1] and Gianlorenzo Franceschina[2]

[1] Istituto Nazionale di Oceanografia e di Geofisica Sperimentale, Centro Ricerche Sismologiche, Via Treviso 55, 33100 Cussignacco, Udine, Italy. E-mails: gbressan@inogs.it, skravanja@inogs.it

[2] Istituto Nazionale di Geofisica e Vulcanologia, Sezione di Milano, Via Bassini 15, 20133 Milano, Italy. E-mail:glf@mi.ingv.it

corresponding author : G. Bressan, e-mail: gbressan@inogs.it, fax +39 0432 522474

Abstract

The source parameters of the major events of a swarm and of two seismic sequences, occurred in the Friuli area (North-eastern Italy) and in Western Slovenia, were estimated. The Claut swarm (C96) occurred since the end of January to June 1996, with a M_D 4.3 major shock and it appears composed of 3 sub-sequences. The two sequences are the Kobarid sequence (K98) started on April, 12, 1998 with a M_D 5.6 mainshock and the M.te Sernio (S02) sequence caused by the February, 14, 2002 earthquake (M_D =4.9). Acceleration and velocity data recorded by the local seismic network of the Istituto Nazionale di Oceanografia e di Geofisica Sperimenale (OGS) and corrected for attenuation, were employed to estimate seismic moments and radiated energies. Source dimensions were inferred from the computed corner frequencies and the stress release was estimated from the Brune stress drop, the apparent stress and the RMS stress drop. On the whole, seismic moments range from 1.7 x 10^{12} to 1.1 x 10^{17} Nm, and radiated energies are in the range 10^6 – 10^{13} J. Brune stress drops are scattered and do not show any evidence of a self-similarity breakdown for sources down to 130 m radius. The radiated seismic energy scales as a function of seismic moment, with a slope of the scaling relation that decreases for increasing seismic moments.

The mechanism of stress release was analyzed by computing the ε parameter of Zuniga (1993). The K98 and S02 sequences are characterized by a wide range of the ε parameter with stress drop mechanism varying from partial locking to overshoot cases. The ε values of the C96 swarm are more homogeneous and close to the Orowan's condition. The radiated seismic energy and the ratio of stress drop between mainshock and aftershocks appear different among the analyzed cases. We therefore investigated the relationship between the stress parameters of the main shock and the energy radiated by the aftershock sequences. For this purpose, we also estimated the source parameters of two other sequences occurred in the area, with mainshocks of M_D 4.1 and M_D 5.1,

respectively. We found a positive correlation between the Brune stress drop of the mainshock and the ratio between the radiated energy of the mainshock and the summation of the energies radiated by the aftershocks.

Key words: earthquakes, seismic sequences, source parameters, scaling law, stress drop

1. Introduction

Earthquake source parameters have been widely used for computing scaling laws exploitable for seismic hazard prediction. A fundamental measure of the earthquake size is the radiated seismic energy, scaled with parameters estimating the stress release, as the stress drop, the apparent stress, the dynamic stress drop, etc. (Choy and Boatwright, 1995; Abercrombie, 1995, McGarr and Fletcher, 2002 and many others). The most frequently used scaling parameter is the stress drop, because it can provide information about the earthquake mechanics. Most of the observational studies in the seismological literature investigated scaling relationships characterizing different seismic areas and different seismotectonic environments or some particular pattern of seismicity (Cocco and Rovelli, 1989; Somerville et al, 1987). An interesting application of source parameters estimation uses seismic sequences to investigate the stress levels, the radiated energy and the mechanism of stress release (Archuleta et al., 1982; Fletcher and Boatwright, 1991; Mori et al., 2003).

In the present study, we analyze the source parameters of two seismic sequences and of a swarm (Fig.1) that occurred in the Friuli area (Northeastern Italy) and in Western Slovenia, characterized by different modes of energy released. The swarm (C96) occurred in the western part of the Friuli-Venezia Giulia region since the end of January to June 1996 with main episodes on January, 27 (M_D 3.5), on February, 27 (M_D 3.8) and on April, 13 (M_D 4.3). The S02 sequence followed the mainshock occurred on February, 14 2002 (M_D 4.9) in the central part of the area, while the K98 sequence followed the mainshock occurred on April, 12 1998 (M_D 5.6) in the western Slovenia.

Two other sequences that occurred in the same area were considered for comparison purposes. The location of these sequences is depicted in Fig. 2. One sequence followed the M_D 4.1 mainshock occurred on May, 28 1998; the other started on July, 12 2004 with the M_D 5.1 mainshock in the Western Slovenia.

The swarm and the seismic sequences are located in areas with different tectonic structure (Fig.3).

The tectonic framework of the area is complex because it results from the superposition of several tectonic phases. The main pre-existing faults, inherited and then reactivated during the different tectonic phases, fragmented the crust into different tectonic domains which form at present different seismotectonic zones (Bressan et al., 2003). The structural setting (Fig.3) in the central and western part of the area consists mainly of E-W trending system of south-verging thrusts and folds, with a few backthrusts and NE-SW oriented thrusts. Strike-slip and normal faults, trending about NW-SE and NNE-SSW intersect the main thrusts. The dominant tectonic structures in the eastern part are NW-SE oriented strike-slip faults and thrusts.

According to historical studies (Camassi and Stucchi, 1997), between 1348 to 1976, this area has experienced destructive earthquakes with at least nine documented earthquakes of intensity greater than or equal to IX in the Mercalli-Cancani-Sieberg scale, alternating with more or less long periods of minor seismicity. The last strong seismic sequence affected northeastern Italy during the period 1976-1977, with a M_W 6.4 mainshock and six events with M_W ranging from 5.1 to 6.0 (Barbano et al., 1985). The present-day seismic activity, recorded from 1977 by the local short-period seismic network of the Istituto Nazionale di Oceanografia e di Geofisica Sperimentale (OGS), affects mainly the central part of the area with localized clusters in the western part of the area and in the Western Slovenia (Franceschina et al., 2006). The mainshocks considered here are the strongest episodes since 1978.

2. Methods

2.1 Locations and magnitudes

In this study, we estimated seismic moment, radiated seismic energy, Brune stress drop, apparent stress and RMS (Root Mean Square) stress drop, adopting the ω^{-2} source model of Brune (1970, 1971) and of Boatwright (1980).

The earthquakes were located with the HYPO71 program (Lee and Lahr, 1975). The crustal model used for the earthquake location consists of two layers and a half-space (depth 0-22 km with Vp=5.85 km/s; depth 22-39.5 km with Vp=6.8 km/s; depth > 39.5 km with Vp=8.0 km/s; Vp/Vs=1.78). The hypocenters were located in the range 4.3 – 15.8 km. The GAP (largest azimuthal separation between stations) was less than 134° (average value 95°), the average horizontal and vertical errors were 0.6 and 1.2 km, respectively.

The HYPO71 locations in the Friuli-Venezia Giulia region were compared with the relocations obtained from the 3-D Vp-Vs tomographic model of Gentile et al. (2000). The average differences in the locations are 2.4 km for the Claut swarm and 1.5 km for the Sernio sequence. The sequence occurred in western Slovenia was located also with the arrival times of permanent and temporary stations of the Seismological Survey of Slovenia, provided by Zivcic et al. (2000). Zivcic et al. (2000) performed a relocation of the sequence with the Joint Hypocentres Determination (JHD) method, used also by Bajc et al. (2001) in their analysis of the 1998 sequence. The comparison between our locations and these relocations gives an average difference of 2.3 km.

The duration magnitude M_D was computed according to Rebez and Renner (1991).

2.2 Seismic sequences and focal mechanisms

The focal mechanisms were computed using the P-wave first motion (Whitcomb, 1973), using also polarity data of seismic stations outside the Friuli-Venezia Giulia region from the Bulletin of the International Seismological Centre (ISC, 2005). The focal mechanisms of

the major events of the swarm and the sequences are taken from Franceschina et al. (2006). The parameters of the fault plane solutions are shown in Tables 1a,b,c,d. Most of the focal mechanisms were calculated using more than 25 polarities. The fault plane solutions are characterized by more than 75% polarities in agreement with the solution obtained. The focal mechanisms of major earthquakes analyzed in the present study are shown in Fig. 4.

The aftershocks were selected moving a 30 days time window, with one day bin and starting two or three months before the mainshock, until the rate (number of events per day) after the mainshock becomes constant. The selection was performed for different radii (distance) from the epicenter of the mainshock.

The aftershock temporal decay is computed with the Utsu's (1961) modified Omori law:

$$n(t) = k(t+c)^{-p} \tag{1}$$

where $n(t)$ is the number of events per unit t; k is related to the total number of earthquakes, c depends on the rate of activity in the earliest part of the sequence and p is related to the decay of aftershocks (Kisslinger and Jones, 1991). The results are summarized in Table 2.

2.3 Spectral analysis

The displacement amplitude spectrum of the SH pulse were assumed as:

$$D(R,f) = \frac{F_s \cdot R_{\theta\phi}}{4\pi\rho\beta^3} \cdot \frac{M_0}{1+(\frac{f}{f_c})^2} \cdot \frac{1}{R} \cdot \exp^{-\pi f\,(K(r)+\frac{R}{\beta Q(f)})} \tag{2}$$

with F_S: free surface correction; $R_{\theta\phi}$: average radiation pattern; ρ: density; β: shear wave velocity; M_0: seismic moment; f_c: corner frequency; R: hypocentral distance. We

assumed F_S = 2 ; ρ = 2.7 g/cm^3 and β =3.3 km/s. The values of the average radiation pattern, $R_{\theta\phi}$, were chosen according to the type of focal mechanisms and to the take-off angles (Boore and Boatwright, 1984). If the focal mechanism was not available, the average coefficient 0.63 was taken. In Eq. (2), the source term is described by the omega-square model of Brune (1970, 1971). The attenuation term includes the spectral decay parameter K of Anderson and Hough (1984) and the quality factor $Q(f)$. The term 1/R accounts for geometrical spreading. The corner frequency f_c was computed following the method of Andrews (1986):

$$f_c = \frac{1}{2\pi}\sqrt{(\frac{S_{v2}}{S_{d2}})} \tag{3}$$

S_{v2} and S_{d2} were calculated by the integrals:

$$S_{v2} = \int_{f_a}^{f_b} V^2{}_{obs}(f)df \tag{4}$$

$$S_{d2} = \int_{f_a}^{f_b} D^2{}_{obs}(f)df \tag{5}$$

where $V_{obs}(f)$ and $D_{obs}(f)$ are the observed amplitude velocity and displacement spectra, respectively. The above integrals were computed between f_a and f_b depending on the noise content of the data. The seismic moment M_0 was then calculated by applying a least-squares algorithm to the displacement amplitude spectrum $D_{obs}(f)$. The f_c and M_0 values were used to calculate the Brune stress drop $\Delta\sigma_B$ and the Brune radius r_B with the relations:

$$\Delta\sigma_B = \frac{M_0 f_c{}^3}{(49\beta)^3} \tag{6}$$

and

$$r_B = \frac{2.34\beta}{2\pi f_c} \tag{7}$$

where $\Delta\sigma_B$, M_0, f_c , β and r_B are expressed in MPa, Nm, Hz, m/s and m respectively.

The radiated seismic energy E_S was computed according to Boatwright (1980):

$$E_S = \frac{2\rho\beta}{e_\beta (F_S R_{\theta\phi})^2} \cdot \int_{f_a}^{f_b} V^2{}_{obs}(f)df \tag{8}$$

with e_β: dimensionless fractional energy flux for shear waves, here assumed equal to $\frac{1}{2\pi}$ for takeoff angles greater than 15° (Randall, 1973).

The apparent stress σ_a introduced by Wyss and Brune (1968) and the RMS stress drop $\Delta\sigma_{rms}$, proposed by Hanks and McGuire (1981) were computed as:

$$\sigma_a = \rho\beta^2 \cdot \frac{E_S}{M_0} \tag{9}$$

and

$$\Delta\sigma_{rms} = \frac{2.7\rho f_c}{R_{\theta\phi}} \cdot \sqrt{\frac{A_4}{A_2}} \tag{10}$$

respectively (Andrews, 1986).

A_4 and A_2 can be estimated from the acceleration spectrum $A_{obs}(f) = 2\pi f V_{obs}(f)$ by:

$$A_4 = \int_{f_a}^{f_b} \left(\frac{A_{obs}(f)}{F_s}\right)^4 df \tag{11}$$

and:

$$A_2 = \int_{f_a}^{f_b} \left(\frac{A_{obs}(f)}{F_s}\right)^2 df \qquad (12)$$

2.4 Source parameters

The procedure adopted for the source parameters estimation is described in Franceschina et al. (2006). The source parameters were calculated for the mainshock and the strongest aftershocks of the sequences, defined as the aftershocks with M_D smaller than mainshock down to 2.0 degrees for C96, 2.6 degrees for K98 and 2.7 degrees for S02.

We considered only time series collected by the digital acquisition system since 1995 with three-components sensors (ZOU, BAD, CAE, DRE, BOO). Station BAD was equipped with a three-component seismometer (1 Hz natural frequency) and with a Kinemetrics FBA-23 digital accelerometer (natural frequency around 50 Hz). Station BOO was equipped with a 1-Hz vertical component seismometer and with two horizontal components of a digital accelerometer (Kinemetrics FBA-23 since February 1996 and Kinemetrics Episensor since march 1999). The acceleration records have a sampling frequency of 125 Hz. Stations ZOU, DRE and CAE were only equipped with three-component seismometers (1 Hz natural frequency). Velocity records obtained by the OGS network are generally sampled at 62.5 Hz. However, since December 1996, velocity records of station ZOU were sampled at 125 Hz. Velocity records were base-line corrected and band pass filtered with a no-causal 8-poles Butterworth filter, with 0.2 Hz high pass frequency. We set the high-pass frequency to 0.4 Hz for the records affected by low signal-to-noise ratio. The low pass frequency of the filter was set to 25 or 50 Hz, depending on the sampling rate of the data. Acceleration records were base-line corrected and band pass filtered between 0.2 and 50 Hz. The deconvolution with the instrument response was then applied both to acceleration

and to velocity time series to obtain the corrected horizontal components of the ground motion.

Site effects of the 3-D seismic stations were accounted for by performing the H/V spectral ratios analysis (Lermo and Chàvez-Garcia, 1993). We used a variable-length time window on the S-wave pulse and applied a mean smoothing algorithm of 0.5 Hz halfwidth on the amplitude Fourier spectrum.

For the source parameters computation, we selected only stations showing H/V spectral ratios not exceeding the value of 2. Fig.5 shows the 95% confidence limits of the ZOU and BAD spectral ratios, that were retained.

We used corrected acceleration and velocity time series recorded at ZOU and BAD in order to compute the transverse and radial components of the ground motion. The amplitude Fourier spectrum of the SH pulse was then calculated from the transverse component, starting at the S-wave arrival and including the most significant part of the signal.

The data were windowed using a two sided 10% cosine taper and zero padded. Variable-length windows from 1.5 to 6.5 s were chosen, depending on the magnitude and distance of the events.

The attenuation effect was removed from the computed spectra by considering an independent estimate of the quality factor $Q(f)$ and a previously obtained estimate of the spectral decay parameter K. We chosed the attenuating function $Q(f) = 78 f^{0.96}$ obtained by Govoni et al. (1996) using coda waves of 150 local events with magnitude range 2.5 - 4.2, recorded by the short-period OGS local network,.

To remove the effects of the high frequency attenuation, we considered the K vs. hypocentral distance empirical relationships obtained by Franceschina et al. (2006) using events with M_L > 3.0 sampled at 125 Hz. Note that the sampling step of the selected data

allowed us to reliably investigate the seismic waves attenuation up to 40-50 Hz. At each station, M_0, f_c, E_S and $\Delta\sigma_{rms}$ were computed from the amplitude Fourier spectrum corrected for all the attenuation effects. The mean values were then considered as the best estimates of the corresponding earthquake source parameters, and finally used to calculate σ_a, $\Delta\sigma_B$ and r_B.

It is noteworthy that the bandwidth limitations of the observed spectrum can lead to incorrect estimates of f_c, particularly for large events that are characterized by corner frequencies similar to the lowest limit of the available frequency band.

Following Di Bona and Rovelli (1988), we corrected the corner frequencies computed by Eq. (3) for bandwidth limitation effects. However, we applied the correction only to the records of the strongest events (K98 and S02), recorded in the frequency band 0.4-25 Hz. In fact, in order to apply this procedure, it is necessary to assume that real spectra follow the ω^{-2} model with great detail, while in general, this model shows an acceptable fit with observed spectra only over the entire frequency band considered for the analysis. In many cases, due to the presence of distorting effects confined in narrow frequency bands, the application of the correction suggested by Di Bona and Rovelli (1988) produces unreliable "corrected" corner frequencies (Franceschina et al., 2006).

Fig. 6b, showing the signal and noise displacement Fourier spectra observed at stations BAD and ZOU (obtained from acceleration and velocity records, respectively), confirms the good quality of data. A signal-to-noise ratio of about 40 and 75 dB is observed around 0.4 Hz for station BAD and ZOU, respectively.

For this event (M_D=5.6), we obtained a corner frequency of 0.46 Hz, by applying the correction for bandwidth limitation effects to velocity records of station ZOU. The corresponding seismic moment of 1.1 x 10^{17} Nm (inferred by the minimization of residuals between the observed and the theoretical displacement spectra), is in good agreement

with the estimate of 3.5 x 10^{17} Nm, obtained from both Harvard CMT solution and inversion of strong motion data (Bajc et al., 2001).

Fig. 6a shows the signal and noise displacement spectra of a typical small event of the analysed dataset (M_D=2.3). BAD station shows the lowest signal-to-noise ratio (about 20 dB between 1 and 3 Hz). However, the corner frequency estimated for this event (f_C=5 Hz), is located within the available frequency band, where a more favourable signal-to-noise ratio is observed.

Fig. 7 shows the time series and corresponding SH pulse displacement Fourier spectra, corresponding to the S02 mainshock, with the superimposed theoretical model. For this earthquake (Franceschina et al., 2006) we used station BAD and three additional stations (CSO, LSR, MLN) not available for the analysis of the other events. We estimated M_0 = 8.4 x 10^{15} Nm and f_c = 1.4 Hz by averaging single estimates of the corresponding source parameters obtained at hypocentral distances approximately ranging from 26 to 46 km. After correction for attenuation effects and distance normalization, the spectra recorded at all stations show an acceptable fit with the ω^{-2} source model characterized by the above reported source parameters.

3. Results and discussion

3.1 Locations and cluster characteristics

1.The 1996 Claut swarm (C96). The Claut swarm occurred since the end of January to June 1996. The temporal distribution shows that the swarm is composed of 3 sub-sequences (Fig.8) and it is strongly clustered (Fig.9). The first sub-sequence started on January, 27 with a M_D 3.5 mainshock, and was followed by 24 aftershocks, with M_D ranging from 1.1 to 2.9, most of which occurred during the same day. The events of this

first sub-sequence are located between 6 to 12 km depth, with the mainshock located at 12 km depth.

The second sub-sequence, started on February, 27 and characterized by a M_D 3.8 mainshock (13 km deep), was followed by about 40 aftershocks with M_D ranging from 1.1 to 3.1, located between 4 and 13 km depth. The first day accounted for most of the aftershocks (24), followed by a quick decay of the number of events per day (Fig.8). A period of quiescence before the subsequent sequence, broken only on April, 2 by an M_D 1.8 event, is recognizable.

The mainshock of the last sub-sequence occurred on April, 13, at about 14 km depth, with M_D 4.3 and it was preceded by 3 foreshocks occurred on April 12 (M_D 2.3) and April, 13 (M_D 3.0 and M_D 2.0). The aftershocks were about 70, located between 4 and 13 km depth, with M_D ranging from 0.3 to 3.5. During the first day of the sub-sequence 25 earthquakes occurred, while after it the number of events per day decreased rapidly (Fig. 8). Minor isolated episodes occurred on May and June. The p values of the Omori's law (Tab.2), that account for the decrease in aftershock activity, show that the decay of the second sub-sequence is faster (p=1.0) than that of the third sub-sequence (p=0.9) and that of the first sub-sequence (p=0.8).

The focal mechanisms of the strongest shocks of the swarm of the 3 sub-sequences are characterized by thrusting, in one case with a strike-slip component, with variable orientation of the nodal planes (Fig.9). They are concordant with the main thrust that affects the area (Fig.3), characterized by planes striking N80°-N130°E and dipping at 40° to 60° to the north (Bressan et al., 2003). The focal mechanisms of the other events show prevailing normal and strike-slip motions, with different nodal plane orientations. A reasonable interpretation comes from Mendoza and Hartzell (1988), who claimed that the fault mechanisms of the aftershocks are influenced by the stress readjustment to the co-seismic slip on the main shock fault. The stress redistribution can cause locally a re-

orientation of the principal axes of stress and therefore can trigger aftershocks with focal mechanisms different from that of the mainshock. Heterogeneities in the physical properties of rocks (Yamashita and Knopoff, 1987) may favour this behaviour.

2. The 1998 Kobarid sequence (K98). The sequence started with a M_D 5.6 mainshock, located at 7.7 km depth, on April, 12, 1998 and lasted till the end of September 1998. The about 700 aftershocks of the sequence (M_D ranging from 1.5 to 4.6) are mainly located between 4 and 10 km depth and define a NW-SE elongated zone. The number of events per day was high during the early 3-4 days (Fig. 10). The decay of the aftershock activity is characterized by p=0.8 (Tab. 2), a low value if compared to the p values (0.6-1.55) of well documented sequences quoted by Utsu et al. (1995).

The mainshock is characterized by a strike-slip focal mechanism (Fig. 11) consistent with the dominant tectonic structure of the area (Fig.3), a set of dextral strike-slip segments, about NW-SE oriented (Bajc et al., 2001). The great variety of the fault plane solutions and the different oriented planes suggest that most of the aftershocks were caused by movement on secondary faults, rather than on a continuous fault surface. The aftershocks characterized by a prevailing normal slip motion could be related to the minor system of NNW-SSE oriented normal faults, bordering the dextral strike-slip segments, recognized by Poli and Renner (2004). Some aftershocks show thrust faulting in agreement with N-NE dipping thrusts, intersected by the strike-slip main faults. Less events with strike-slip motion are also present.

3. The 2002 M.te Sernio sequence (S02). The mainshock (M_D 4.9) occurred on February, 14, 2002 at about 13 km depth, preceded five minutes before by a M_D 2.5 foreshock. The sequence lasted till the end of June 2002 and consisted of about 60 events, mainly located between 7 and 10 km depth with the M_D ranging between 0.4 and 3.2. The number of aftershocks was about 20 during the first day, while in the following days the number of earthquakes per day quickly decayed (Fig.12). The p value of the Omori's regression is 0.8

(Tab.2). Some periods of quiescence appear during the aftershock sequence. The events of the sequence are partly scattered and partly clustered around the mainshock (Fig.13). The focal mechanism of the mainshock shows a prevailing thrusting, with a small strike-slip component, the same mechanism that characterizes the foreshock. The two shocks appear related to a thrust striking about E-W and dipping about 40 °to the N-NNE. The dominant tectonic structures in this area (Fig.3) are E-W trending thrusts and backthrusts, displaced in some points by minor vertical faults which bend N140°-150°E and N20°-30°E (Bressan et al., 2003). The fault plane solutions of the strongest aftershocks refer mainly to thrusting mechanisms with variable nodal planes orientation and to a minor episode with normal motion.

As pointed out before, the variability in the strike of the nodal planes and in some cases of the type of focal mechanisms during an aftershock sequence can be explained according to Mendoza and Hartzell (1988). Furthermore, King at al. (1994) demonstrated that the shear stress changes caused by coseismic displacement, in addition to the regional deviatoric stress, control the orientation of optimal fault planes for Coulomb failure conditions.

As quoted in the introduction, two other sequences are considered only for comparison purposes (Fig. 2). One occurred on May, 28 1998 near the village of Trasaghis with a M_D 4.1 mainshock (T98), followed by 17 aftershocks with M_D ranging from 0.8 to 2.9, within 2 months after the mainshock. The other sequence started on July, 12, 2004 in the Kobarid area, close to the hypocenter of the April, 12, 1998, M_D 5.6 event. The mainshock (K04), with M_D 5.1, was followed by about 300 aftershocks until December 2004, with M_D ranging from 1.0 to 3.6.

The Trasaghis mainshock (T98) shows a reverse focal mechanism (Fig. 4) related to south-verging thrusts and is located at about 11 km depth. The aftershocks are located between 7 and 12 km depth. The K04 mainshock is located at about 7.6 km depth, and it

is characterized by a strike-slip focal mechanism, very similar to that one of the April, 12, 1998 mainshock (Fig. 4), and related to strike-slip faulting. According to the simple model used, the depths of the aftershocks are in the range 4 – 10 km.

3.2 Source parameters and scaling

The source parameters of the C96 swarm and of the K98 and S02 sequences are listed in tables 3, 4, and 5, respectively. These tables report also the maximum and minimum values, the multiplicative error of the lognormal distribution of each source parameter and the average values of the stress parameters. The parameters of the C96, K98 and S02 mainshocks and of 12 aftershocks of the K98 sequence are taken from Franceschina et al. (2006). C96, K98 and S02 earthquakes present different ranges of hypocentral distance. The hypocentral distances of the S02 events range from about 18 to 30 km from both ZOU and BAD stations. The C96 swarm, more clustered with respect to the sequences, is characterized by average hypocentral distances from ZOU and BAD equal to 43 and 54 km, respectively. The K98 earthquakes were recorded at average hypocentral distances of about 60 km from station ZOU and of 34 km from station BAD.

The range of the estimated seismic moments is 10^{12} - 10^{17} Nm. The measured corner frequencies correspond to Brune source radii ranging from about 130 to 2700 m, in agreement with the global scaling of source parameters in this region (Franceschina et al., 2006). For the analysed sequences, the mean multiplicative errors do not exceed 1.3 and 1.5 for corner frequencies and seismic moments, respectively. The latter corresponds to an uncertainty of 0.17 on the logarithm of the seismic moment, a value similar to the station corrections for the local magnitude calibration in Northeastern Italy (Bragato and Tento, 2005). Fig.14 shows the seismic moments of the analyzed sequences versus Brune radii, with lines of constant stress drop.

A general increase of the fault radius with increasing seismic moment and a lack of correlation between $\Delta\sigma_B$ and M_0 can be observed. This behaviour could be consistent with a global constant stress drop scaling law in the seismic moment range 1.7 x 10^{12} - 1.1 x 10^{17} Nm, down to 0.13 km fault radius.

The large scatter of the $\Delta\sigma_B$ values is probably due to the cubed-sized dependence of the stress drop on corner frequency, and consequently, it is linked to the variability of the estimated source dimensions. In fact, corner frequency estimates can be affected by azimuth dependent propagation effects, site effects and source directivity.

As a result of the cubed-sized dependence of $\Delta\sigma_B$ on f_c, we obtain mean multiplicative errors of the order of 2 for the Brune stress drop.

The radiated seismic energies, E_S, are in the range of 10^6 - 10^{13} J, with differences among the sequences and the swarm that reflect the corresponding difference of seismic moment ranges. Seismic energies, are plotted against the seismic moments in Fig. 15, with lines of constant apparent stress. Multiplicative errors affecting both E_S and σ_a estimates range between 3 and 4. The seismic energy increases with seismic moment according to the following relations:

C96: $\log E_S = 1.7 \log M_0 - 14.1$; $\sigma(\log E_S)=0.3$; $M_0=1\text{x}10^{12}–1\text{x}10^{15}$ Nm

K98 : $\log E_S = 1.2 \log M_0 - 8.4$; $\sigma(\log E_S)=0.4$; $M_0=2\text{x}10^{13}–2\text{x}10^{17}$ Nm (13)

S02: $\log E_S = 1.4 \log M_0 - 11.0$; $\sigma(\log E_S)=0.3$; $M_0=2\text{x}10^{12}–9\text{x}10^{15}$ Nm

where E_S and M_0 are expressed in J and Nm respectively. It is noteworthy that the slope of the scaling relations decreases as the seismic moment increases.

The apparent stress increase as a function of M_0 can also be described in terms of a larger ratio of radiated energy to seismic moment for larger earthquakes. As a possible explanation of this, Mori et al. (2003) claimed that the larger events tend to be more

complex and characterized by greater high-frequency content, therefore radiating more energy.

Also the analysis of the 53 local earthquakes (2.0 < ML < 5.6) performed by Franceschina et al. (2006), and a recent study investigating the scaling relations for small earthquakes (-1.8 < M_W < 1.2) recorded at 1.4 km depth (Oye et al., 2005), show an increase of the apparent stress with increasing M_0 , together with an apparently constant stress drop. In these studies, the $\Delta\sigma_B$ and σ_a different scalings were both accommodated by the modified $M_0 \sim f_C^{-(3+\varepsilon)}$ scaling relation of Kanamori and Rivera (2004).

As in Franceschina et al. (2006), we exclude an underestimation of E_S due to the bandwidth limitation effects. Franceschina et al. (2006), by applying the correction suggested by Ide and Beroza (2001) to events with similar magnitude and recorded by the same stations, found a negligible change in the slope of the energy - moment scaling relation (from 1.30 to 1.26).

As explained in the introduction, we compared the location of the earthquakes obtained with the HYPO71 program with the location obtained with the 3-D Vp-Vs tomographic model of Gentile et al. (2000) for C96 and S02 events, and with the JHD method (Zivcic et al, 2000) for K98 events. The average difference distances from recording stations used in the present work are for C96 events: 0.7 km (ZOU) and 0.3 km (BAD); for K98 events: 0.8 km (ZOU) and 0.7 km (BAD); for S02 events: 0.8 km (ZOU) and 0.3 km (BAD). However, being the maximum observed difference of 2.6 km, we consider negligible the influence of the location method on the estimate of the source parameters. In fact, due to the small value of dK/dR for both stations ZOU and BAD (see Eqs.(16) and (17) in Franceschina et al., 2006), this difference does not affect the estimate of the spectral decay parameter K , and consequently, of the corner frequency. Moreover, due to the combined effects of

geometrical spreading and of the quality factor (see Eq.(1)), this difference implies a 11% increase of M_0 and a 14% increase of E_S. From Eqs. (5) and (8), it follows that $\Delta\sigma_B$ and σ_a increase of 11% and 4%, respectively.

The RMS stress drop values, $\Delta\sigma_{rms}$, are generally higher than the other stress parameters. $\Delta\sigma_{rms}$ is characterized by multiplicative errors between 3 and 5, and appears to be not correlated with M_0 (Fig.16).

3.3 Stress release

Besides the above mentioned differences of the average values of the estimated source parameters, the sequences here analyzed show differences in the mechanism of stress release. Table 3 shows that the $\Delta\sigma_B$ values of the C96 swarm are characterized by high variability. Tables 4 and 5 evidence that most of the K98 and S02 aftershocks show low stress drops compared to that of the mainshock, and this behaviour is particularly marked for S02. These aftershocks could result from low residual stresses after the mainshock rupture. As regard to foreshocks, it is noteworthy that both C96 and S02 are characterized by low stress drop of the foreshocks relative to that of the mainshocks (n.12 of tab. 3 and n.1 of tab. 5). This could suggest that the foreshocks nucleated on the weaker parts of the mainshock rupture plane.

Different modes of stress release among C96, K98 and S02 are also suggested by the temporal differences in the events occurrence clearly recognizable from Figs. 5, 7 and 9. In fact, the C96 swarm appears composed of three sub-sequences, and the S02 sequence is characterized by some periods of quiescence during the aftershock occurrence.

Moreover, Fig. 15 evidences the different ranges of the energy released by the aftershocks of the analyzed sequences: 10^6 - 10^9 J for C96; 10^7 - 10^{10} J for K98 and 10^6 – 10^8 J for S02.

Finally, it is noteworthy that, despite the K98 mainshock has a seismic moment larger than the S02 mainshock, the $\Delta\sigma_B$ of S02 mainshock is twice the $\Delta\sigma_B$ of the K98 mainshock (see tables 4 and 5).

In order to investigate the mechanism of stress release we also computed the ε parameter of Zuniga (1993), defined as:

$$\varepsilon = \frac{\sigma_1 - \sigma_2}{\sigma_1 - \sigma_f} = \frac{\Delta\sigma}{\sigma_a + \frac{\Delta\sigma}{2}} \qquad (14)$$

where σ_1 , σ_2 and σ_f represent the initial, the final and the frictional stress respectively , while σ_a and $\Delta\sigma$ represent the apparent stress and the stress drop, respectively. We computed ε assuming $\Delta\sigma = \Delta\sigma_B$.

Conditions of partial stress drop (partial locking) result if the final stress is greater than the frictional stress (ε < 1). The faulting model of Orowan (1960) results if the final stress is equal to the frictional stress (ε = 1). The case with final stress lower than the frictional stress is named the overshoot case (ε > 1).

Tables 3, 4 and 5 summarize the obtained ε values while Figs. 17, 18 and 19 show the ε trend as a function of time. The C96 swarm (Fig. 17) is characterized by a homogeneous distribution of the ε values (between 1.0 and 1.1), close to the model of Orowan (1960). On the contrary, the K98 (Fig. 18) and S02 (Fig. 19) sequences are characterized by scattered ε values, alternating from partial locking to overshoot cases. For both sequences the range of variation of this parameter is approximately 0.5 - 1.5, and the partial locking effect (ε < 1) is slightly larger for the K98 mainshock with respect to the S02 mainshock. However, great caution must be used in interpreting these results.

In fact, as a consequence of the uncertainties affecting both σ_a and $\Delta\sigma_B$, the estimated ε values are affected by large errors (being the multiplicative errors for both K98 and S02 ε values nearly equal to 5 and for C96 equal to 3.6).

Probably, most of the above mentioned features are related to the mechanism of stress release of the main event of each sequence, which is clearly identifiable for S02 and K98 only. As already mentioned, most of the S02 and K98 aftershocks are characterized by lower stress drop than the mainshock. However, this characteristic is particularly evident for the S02 sequence. In fact, the ratio between the $\Delta\sigma_B$ of the mainshock and the mean value of the aftershocks stress drops, R_{SD} , is 4.9 and 9.2 for K98 and S02 respectively. The K98 aftershocks also show a wider range of stress drop values, with some value comparable with that of the mainshock.

The different modes of energy and stress release between K98 and S02 sequences can thus be summarized as follows:

1) M_0 (S02 mainshock) < M_0 (K98 mainshock)
2) E_S (S02 mainshock) < E_S (K98 mainshock)
3) E_S – range (S02 aftershocks) < E_S – range (K98 aftershocks)
4) $\Delta\sigma_B$ (S02 mainshock) > $\Delta\sigma_B$ (K98 mainshock)
5) R_{SD} (S02) > R_{SD} (K98)

While features summarized by points 1, 2 and 3 are simply connected to the different source dimensions of the S02 and K98 mainshocks, the properties related to points 4 and 5 could probably reflect a different mechanism of stress release between these two sequences, suggesting that the residual stresses, after the mainshock rupture, could be higher in K98 than in S02.

According to Scholz (1990), the aftershocks result from the stress readjustment following the mainshock faulting. Therefore, they are considered a secondary process caused by the residual stresses remaining after the mainshock rupture. This suggests that the stress released by the mainshock can influence the partition of seismic energy between mainshock and aftershocks. Following this hypothesis, we computed for each sequence the parameter R_{ES} defined as the ratio between the energy radiated by the mainshock and the summation of the energies radiated by the aftershocks. For this analysis we considered the T98 and the K04 while the 3 sub-sequences that compose the C96 swarm are considered as distinct sequences.

For all sequences we retained the aftershocks with $M_D \geq 2.0$ and computed E_S using an empirical relation between the duration magnitude and the radiated seismic energy. The adopted relation is: $\text{Log } E_S = 1.94\ M_D + 2.26$, resulting from the analysis of the Franceschina et al. (2006) dataset.

Tab. 6 shows the source parameters of the mainshocks of all the analyzed sequences with the ratio R_{ES} between the energy radiated by the mainshock and the summation of the energies radiated by the aftershocks. Multiplicative errors of this parameter are typically of the order of 4.

Since our interest was focussed on the influence of the mainshock stress release on the partition of seismic energy between mainshock and aftershocks, we considered the source stress parameters in relation to R_{ES} . The best correlated source parameter is $\Delta\sigma_B$, that appears to increase with R_{ES}, or better, the higher the main shock $\Delta\sigma_B$ is, the lower is the total energy radiated by the aftershocks with respect to the energy radiated by the mainshock. Fig. 20 shows the linear fit obtained by regression of R_{ES} versus $\Delta\sigma_B$ data.

Even if a full treatment of the relationships between the stress release and the mechanics of earthquake rupture is beyond the scope of the present paper, some considerations can be done.

As discussed in Franceschina et al. (2006), the stress drop parameter may be variously interpreted. Atkinson and Beresnev (1996) emphasized that the physical meaning of the stress drop has been characterized in literature by ambiguities and non univocal interpretations and they pointed out that the most suitable definition of stress drop is that of a measure of slip relative to fault dimension. According to Boatwright (1984), the Brune stress drop is an effective stress, that is the difference between initial stress and fault friction stress while the fault is slipping. Zuniga et al. (1987) and Feignier and Grasso (1991) related the stress drop to the strength of rocks. As a consequence, higher strength could lead to large stress concentrations and maximal stress drops are related to the maximum state of stress each rock can sustain. However, despite the ambiguities evidenced by Atkinson and Beresnev (1996), the Brune stress drop can be considered as a source parameter reflecting relative changes in stress. The positive correlation between $\Delta\sigma_B$ and the ratio between the radiated energy of the mainshock and the summation of the radiated energy of the aftershocks suggests that the higher is the Brune stress drop of the mainshock, the lower are the residual stresses remaining in the focal volume, causing events with lower radiated energy.

4. Conclusions

We computed the source parameters of the major events of two seismic sequences, Kobarid 1998 (K98) and M.te sernio 2002 (S02) and of a swarm, Claut 1996 (C96), occurring in the Friuli area (Northeastern Italy) and in Western Slovenia. The main conclusions can be summarized as follows:

- The C96 swarm appears composed of 3 sub-sequences with different decrease in aftershock activity. The P values of the Omori's law are 0.8, 1.0 and 0.9, respectively. The K98 and the S02 aftershock decays are both characterized by P = 0.8.
- The $\Delta\sigma_B$ values are consistent with a constant stress drop scaling law down to 130 m fault radius, for seismic moments ranging 10^{12} – 10^{17} Nm.
- The analyzed sequences and the swarm are characterized by a different increase of the radiated seismic energy with the seismic moment. The differences reflect the corresponding differences of seismic moment ranges. The slope of the scaling relation E_S - M_0 decreases as the seismic moment increases and, consequently, apparent stress increases as a function of M_0.
- Both σ_a and $\Delta\sigma_B$ scalings can be accommodated by the modified $M_0 \sim f_C^{-(3+\varepsilon)}$ scaling relation of Kanamori and Rivera (2004), as discussed in Franceschina et al. (2005).
- The RMS stress drop values are generally higher than the other stress parameters and are not correlated with the seismic moment.
- The ε parameter proposed by Zuniga (1993) to investigate the variations in stress drop mechanism, shows a homogeneous distribution for the C96 swarm, with values 1.0 and 1.1, close to the Orowan's condition. More scattered values characterize the K98 and the S02 sequence, varying from partial locking (ε < 1) to overshoot (ε > 1) cases.
- With respect to the S02 mainshock, the K98 mainshock shows a larger seismic moment but a lower $\Delta\sigma_B$. Most of the S02 aftershocks show a low stress drop compared to the mainshock, while a wide range of $\Delta\sigma_B$ values characterizes the K98 aftershocks. The ratio between the $\Delta\sigma_B$ of the mainshock and the mean value of the aftershocks stress drops is 4.9 and 9.2 for K98 and S02 respectively. Two

recognized foreshocks have a relatively low stress drop, indicating that they probably nucleated on the weaker part of the main fault rupture.

- The energy distribution of the analyzed sequences was investigated introducing the ratio R_{ES} between the energy radiated by the mainshock and the summation of the energies radiated by the aftershocks. We included in this analysis two other sequences following two shocks with M_D 4.1 and M_D 5.1, occurred in the area. For all the analyzed sequences, R_{ES} was observed to increase with the $\Delta\sigma_B$ of the mainshock, suggesting that the higher is the Brune stress drop of the mainshock, the lower are the residual stresses remaining in the focal volume, causing events with lower radiated energy.

Acknowledgments

The local seismic network is managed by the Dept. Centro di Ricerche Sismologiche of Istituto Nazionale di Oceanografia e di Geofisica Sperimentale (OGS) with financial contribution of the Regione Friuli-Venezia Giulia. We are grateful to S. Gentili for her helpful contribution about the seismic sequences analysis. We thank P. Bragato who performed data management and S. Urban for help in graphics. Thanks are due also to the technical staff for data acquisition.

References

Abercrombie, R.E., 1995. Earthquake source scaling relationships from -1 to 5 M_L using seismograms recorded at 2.5 – km depth. J. Geophys. Res., 100: 24015-24036.

Anderson, J.G., and Hough, S., 1984. A model for the shape of Fourier amplitude spectrum of acceleration at high frequencies. Bull. Seismol. Soc. Am., 74: 1969-1994.

Andrews, D.J., 1986. Objective determination of source parameters and similarity of earthquakes of different size. In S. Das, J. Boatwright, and C. H. Scholz (Editors) Earthquake Source Mechanics, Am. Geophys. Union, Geophys. Monogr. Ser., 6: 259-267.

Archuleta, R. J., Cranswick, E., Mueller, C., and Spudich, P. 1982. Source parameters of the 1980 Mammoth Lakes, California, earthquake sequence. J. Geophys. Res., 87: 4595-4697.

Atkinson, G.M., and Beresnev, I., 1997. Don't call it stress drop. Seismol. Res. Lett.. 68: 3-4.

Bajc, J., Aoudia, A., Saraò, A., and Suhadolc, P., 2001. The 1998 Bovec-Krn mountain (Slovenia) earthquake. Geophis. Res. Lett., 28, 1839-1842.

Barbano, M. S., Kind, R. & Zonno, G. 1985. Focal parameters of some Friuli earthquakes (1976-1979) using complete theoretical seismograms. *J. Geophys.*, **58**, 175-182.

Boatwright, J., 1980. A spectral theory for circular seismic sources: simple estimates of source dimension, dynamic stress drop and radiated energy. Bull. Seismol. Soc. Am., 70: 1-27.

Boatwright, J., 1984. Seismic estimates of stress release. J. Geophys. Res., 89: 6961-6968.

Boore, D.M., and Boatwright, J., 1984. Average body-wave radiation coefficients. Bull. Seismol. Soc. Am., 74: 1615-1621.

Bragato, P.L., and Tento, A., 2005. Local magnitude in Northeastern Italy. Bull. Seismol. Soc. Am., 95, 579-591.

Bressan, G., Bragato, P.L., and Venturini, C., 2003. Stress and strain tensors based on focal mechanisms in the seismotectonic framework of the Friuli-Venezia Giulia region (Northeastern Italy). Bull. Seismol. Soc. Am., 93, 1280-1297.

Brune, J.N., 1970. Tectonic stress and the spectra of seismic shear waves from earthquakes. J. Geophys. Res., 75: 4997-5009.

Brune, J.N., 1971. Correction. J. Geophys. Res., 76: 5002.

Camassi, R., and Stucchi M., 1997. NT4.1. Un catalogo parametrico di terremoti di area italiana al di sopra della soglia del danno, GNDT, Milano, 66 pp.

Choy, G. L. and Boatwright, J. L., 1995. Global patterns of radiated seismic energy and apparent stress, J. Geophys. Res., 100: 18205-18228.

Cocco, M. and Rovelli, A. 1989. Evidence for the variation of stress drop between normal and thrust faulting earthquakes in Italy. J. Geophys. Res., 94: 9399-9416.

Di Bona, M., and Rovelli, A., 1988. Effects of the bandwidth limitation on stress drops estimated from integrals of the ground motion. Bull. Seismol. Soc. Am., 78: 1818-1825.

Feignier, B., and Grasso, J.R., 1991. Relation between seismic source parameters and mechanical properties of rocks: a case study. Pure Appl. Geophys. ,137: 175-199.

Fletcher, J. B. and Boatwright, J. 1991. Source parameters of Loma Prieta aftershocks and wave propagation characteristics along the San Francisco peninsula from a joint inversion of digital seismograms. Bull. Seism. Soc. Am., 81: 1783-1812.

Franceschina, G., Kravanja, S. and Bressan G., 2006. Source parameters and scaling relationships in the Friuli-Venezia Giulia (Northeastern Italy) region. Phys. Earth Planet. Inter., 154: 148-167.

Gentile, G. F., G. Bressan, L. Burlini, and R. De Franco, 2000. Three – dimensional Vp and Vp/Vs models of the upper crust in the Friuli area (Northeastern Italy). Geophys. Journ. Int.,141, 457-478.

Govoni, A., Bragato, P.L., and Bressan, G., 1996. Coda Q_C evaluation using local seismic events in the Friuli area, Atti del 15° Convegno G.N.G.T.S., Roma, Italy, 389-392.

Hanks, T., and McGuire, T., 1981. The character of high-frequency strong ground motion. Bull. Seismol. Soc. Am., 71: 2071-2095.

Ide, S., and Beroza, G.C., 2001. Does apparent stress vary with earthquake size ?. Geophys. Res. Lett., 28: 3349-3352.

ISC, 2005. Bulletin of the International Seismological Center, http://www.isc.ac.uk (last accessed April 2005).

Kanamori, H. and Rivera, L., 2004. Static and dynamic scaling relations for earthquakes and their implications for rupture speed and stress drop. Bull. Seismol. Soc. Am., 94: 314 -319.

King, G.C.P., Stein, R.S. and Lin, J., 1994. Static stress changes and the triggering of earthquakes, Bull. Seismol. Soc. am., 84: 935-953.

Kisslinger, C., and L. M. Jones,1991. Properties of aftershock sequences in Southern California. Journ. Geophys. Res., 96, 11947-11958.

Lee, W.H.K., and Lahr, J.C., 1975. HYPO71 (revised); a computer program for determining hypocenter, magnitude and first motion pattern of local earthquakes. U.S. Geol. Surv. Open-File Rept., 75-311, 113 pp.

Lermo, J., and Chàvez-Garcìa, F.C., 1993. Site effect evaluation using spectral ratios with only one station. Bull. Seismol. Soc. Am., 83: 1574-1594.

McGarr, A. , and Fletcher, J. B., 2002. Mapping apparent stress and energy radiation over fault zones of major earthquakes. Bull. Seismol. Soc. Am., 92: 1633-1646.

Mendoza, C., and Hartzell, S.H., 1988. Aftershock patterns and main shock faulting. Bull. Seismol. Soc. Am., 78, 1438-1449.

Mori, J., Abercrombie, R. E., and Kanamori, H., 2003. Stress drops and radiated energies of aftershocks of the 1994 Northridge, California, earthquakes. J. Geophys. Res., 108(B11), 2545, doi:10.1029/2001JB00474.

Oye, V., Bungum, H., and Roth, M., 2005. Source parameters and scaling relations for mining-related seismicity within the Pyhäsalmi ore mine, Finland. Bull. Seismol. Soc. Am., 95: 1011-1026.

Orowan, E., 1960. Mechanism of seismic faulting. Geol. Soc. Am., 79: 323-345.

Poli, M. E., and Renner, G., 2004. Normal focal mechanisms in the Julian Alps and Prealps: seismotectonic implications for the Italian-Slovenian border region. Boll. Geof. Teor. Appl., 45, 51-69.

Randall, M.J., 1973. The spectral theory of seismic sources. Bull.Seismol.Soc.Am., 63: 1133-1144.

Rebez, A. and Renner G., 1991. Duration magnitude for the northeastern Italy seismometric network. Boll. Geof. Teor. Appl., 33: 177-186.

Scholz C. H., 1990. The mechanics of earthquakes and faulting. Cambrige University Press, 439 pp.

Somerville, P.G., McLaren, J.P., LeFevre, L.V., Burger R.W., and Helmberger, D.V., 1987. Comparison of source scaling relations of eastern and western north american earthquakes. Bull. Seismol. Soc. Am., 77: 322-346.

Utsu, T.,1961. A statistical study on the occurrence of aftershocks. Geophys. Mag., 30, 521-605.

Utsu, T., Ogata, Y., and Matsu'ura, R.S., 1995. The centenary of the Omori formula for a decay law of aftershock activity. J. Phys. Earth, 43, 1-33.

Whitcomb, J. H., 1973. Part I. A study of the velocity structure of the Earth by the use of core phases. Part II. The 1971 San Fernando earthquake series, focal mechanisms and tectonics, Ph.D. Thesis, California Institute of Technology, Pasadena, 443 pp..

Wyss, M. and Brune, J. N., 1968. Seismic moment, stress and source dimensions for earthquakes in the California – Nevada region. J. Geophys. Res., 76: 4681-4694.

Yamashita, T., and Knopoff, L., 1987. Models of aftershock occurrence. Geophys. J.R.A.S., 91, 13-26.

Zivcic, M., Govoni, A. and Costa, G., 2000. The 1998 Krn Mountains earthquake sequence. The combined data set of the URSG, OGS and DST temporary and permanent seismic networks (Apr. 12 - Dec. 31, 1998). CD-ROM, Gephysical Survey of Slovenia, Osservatorio Geosico Sperimentale, Dip. Scienze della Terra - Univ. Trieste.

Zoback, M.L., 1992. First- and second-order patterns of stress in the lithosphere: the world stress map project. J. Geophys. Res. 97: 11703-11728.

Zuniga, R., 1993. Frictional overshoot and partial stress drop. Which one?, Bull.Seismol. Soc. Am., 83: 939-944.

Zuniga, F.R., Wyss, M. and Wilson, M.E., 1987. Apparent stresses, stress drops, and amplitude ratios of earthquakes preceding and following the 1975 Hawai M_S = 7.2 main shock. Bull. Seismol. Soc. Am., 77: 69-96.

Figure captions

Fig. 1 – Map of the earthquake sequences. Circles: the 1996 Claut swarm (C96); diamonds: the 1998 Kobarid sequence (K98); triangles: the 2002 M.te Sernio sequence (S02). The focal mechanisms of the mainshocks are plotted with duration magnitude in parenthesis. Black triangles show the location of the seismic stations of the OGS local network. BAD and ZOU are the recording stations used for source parameter estimation. UD: Udine town; PN: Pordenone town; TS: Trieste town. The inset shows the location of the study area. Longitude-degrees (horizontal axis), latitude-degrees (vertical axis).

Fig. 2 - Location of the 1998 Trasaghis sequence (circles) and of the 2004 Kobarid sequence (diamonds). The focal mechanisms of the mainshocks are also shown, with duration magnitude in parenthesis. Other symbols as in Fig.1. Longitude-degrees (horizontal axis), latitude-degrees (vertical axis).

Fig. 3 – Tectonic pattern of the northeastern Italy and Western Slovenia; line and dashed line: subvertical fault, toothed line: thrust. The location of the mainshocks of the sequences considered in the present work are portrayed with different symbols; full circle: 1996 Claut mainshock, full triangle: 2002 M.te Sernio mainshock, star: 1998 Trasaghis mainshock, full square: 1998 and 2004 Kobarid mainshocks. BL: Belluno town; PN: Pordenone town; UD: Udine town; GO: Gorizia town; TS: Trieste town. Longitude-degrees (horizontal axis), latitude-degrees (vertical axis).

Fig. 4 – Focal mechanisms of major earthquakes of the sequences considered in the paper. C96 (1): M_D 3.5 event of 1996 January, 27; C96 (4): M_D 3.8 event of 1996 February, 27; C96 (13): M_D 4.3 event of 1996 April, 13. The number in parenthesis are as in Table 3. K98 (1): M_D 5.6 event of 1998 April, 12; K98 (14): M_D 4.6 event of 1998 May, 6. The number in parentheses are as in Table 4. T98: M_D 4.1 event of 1998 May, 28. S02 (2): M_D

4.9 event of 2002 February, 14; S02 (8): M_D 3.2 event of 2002 February, 25. The number in parentheses are as in Table 5. K04: M_D 5.1 event of 2004 July, 12.

Fig. 5 - 95% confidence limits of H/V spectral ratios obtained from S-waves at stations ZOU and BAD. Dark pattern: N-S component; grey pattern: E-W component.

Fig. 6 – Signal (thick line) and noise (thin line) displacement Fourier spectra observed at stations BAD and ZOU, obtained from acceleration and velocity records, respectively. a) low magnitude event (M_D 2.3, n.3 of Table 5); b) strong magnitude event (M_D 5.6, n.1 of Table 4).

Fig. 7 – Waveforms (left panel) recorded at stations BAD, CSO, LSR, MLN and displacement spectra of the 2002 February 14, mainshock (M_D 4.9) of the S02 sequence. The time series represent the transverse components of velocity and acceleration records, obtained after deconvolution with the instrument response. The grey shaded areas indicate the used time windows. The displacement spectra were corrected for attenuation and normalized at 10 km hypocentral distance. The theoretical spectra (grey line) were computed with the seismic moment and corner frequency values listed in Table 5.

Fig. 8 – Temporal distribution of the 1996 Claut swarm (C96). The duration magnitude of the major earthquakes (M_D greater or equal to 2.8) is also shown (full circles).

Fig. 9 – Map of the 1996 Claut swarm (C96) with fault plane solutions of the largest earthquakes. The focal mechanisms of the major shocks are drawn with larger size. The focal mechanisms are numbered as in Table 3, with duration magnitude in parentheses. The main toponyms are also shown. Longitude-degrees (horizontal axis), latitude-degrees (vertical axis).

Fig. 10 – Temporal distribution of the 1998 Kobarid sequence (K98). The duration magnitude of the major earthquakes (M_D greater or equal to 3.0) is also shown (full circles).

Fig. 11 – Map of the 1998 Kobarid sequence (K98) with fault plane solutions of the largest earthquakes. The focal mechanisms of the mainshock is shown with larger size. The focal mechanisms are numbered as in Table 4, with duration magnitude in parentheses. The main toponyms are also shown. Longitude-degrees (horizontal axis), latitude-degrees (vertical axis).

Fig. 12 – Temporal distribution of the 2002 M.te Sernio sequence (S02). The duration magnitude of the major earthquakes (M_D greater or equal to 2.3) is also shown (full circles).

Fig. 13 – Map of the 2002 M.te Sernio sequence (S02), with fault plane solutions of the largest earthquakes. The focal mechanisms of the mainshock is shown with larger size. The focal mechanisms are numbered as in Table 5, with duration magnitude in parentheses. The main toponyms are also shown. Longitude-degrees (horizontal axis), latitude-degrees (vertical axis).

Fig. 14 – Seismic moment vs. source radius. Lines of constant stress drop are also shown. Full circles: C96 swarm; open circles: K98 sequence; squares: S02 sequence.

Fig. 15 – Radiated seismic energy plotted as a function of seismic moment. Lines of constant apparent stress are also shown. Full circles: C96 swarm; open circles: K98 sequence; squares: S02 sequence.

Fig. 16 – Plot of the RMS stress drop vs. seismic moment. Full circles: C96 swarm; open circles: K98 sequence; squares: S02 sequence.

Fig. 17 - C96 swarm. ε parameter of Zuniga (1993) as a function of time. The full circles indicate the main events of the 3 sub-sequences of the swarm. Numbers refer to the first column of Table 3. Time is measured starting at the first day of the year.

Fig. 18 - K98 sequence. ε parameter of Zuniga (1993) as a function of time. The full circle indicates the K98 mainshock. Time is measured starting at the first day of the year.

Fig. 19 - S02 sequence. ε parameter of Zuniga (1993) as a function of time. The full circle indicates the S02 mainshock. Time is measured starting at the first day of the year.

Fig. 20 – Brune stress drop plotted as a function of the ratio between the energy radiated by the mainshock and the summation of the energies radiated by the aftershocks (R_{ES}), for each sequence considered. The number in parenthesis refer to the first columns of Table 3 (C96), Table 4 (K98) and Table 5 (S02). The dashed line represents the best-fit linear regression: Log R_{ES} = 2.64 Log $\Delta\sigma_B$ + 0.91 ; σ(Log R_{ES}) = 0.39 .

Tables

N	Date	Time	M_D	Az1	Dip1	Rake1	Az2	Dip2	Rake2	FPS	Np	Sc
1	96-01-27	08:26:00.9	3.4	135	47	113	282	48	67	TF	34	0.85
2	96-01-27	08:30:25.5	2.9	213	47	-14	313	80	-136	SS	24	0.91
3	96-01-27	15:28:28.7	3.0	25	52	-92	209	37	-87	NF	18	0.83
4	96-02-27	11:13:45.6	3.8	74	41	92	252	48	88	TF	41	0.87
7	96-02-27	12:38:44.3	2.8	57	56	82	251	34	102	TF	22	0.86
8	96-02-27	13:43:48.4	2.9	306	40	-117	160	54	-68	NF	24	0.75
9	96-02-27	19:47:40.7	2.5	192	47	-67	341	47	-112	NF	17	0.88
13	96-04-13	13:00:22.5	4.3	38	41	36	278	66	125	TF	61	0.86
16	96-04-15	13:07:43.4	2.9	139	76	-58	250	34	-155	NS	25	0.76
17	96-04-16	18:06:51.8	3.7	194	43	-4	288	87	-133	SS	36	0.80
18	96-05-06	10:20:08.5	2.9	54	14	-125	271	78	-81	NF	21	0.95

Tab.1a

Focal parameters of the C96 Claut swarm. N: sequential number as in Table 3. M_D: duration magnitude. Az and Dip are azimuth and dip of the nodal plane. The type of focal mechanisms (FPS) was classified according to Zoback (1992): NF=normal faulting, NS= predominately normal faulting with strike-slip component; SS=strike-slip faulting; TS=predominately thrust faulting with strike-slip component; TF=thrust faulting. Np is the polarity number used for elaborating the focal mechanisms. Sc (score) is the ratio between the number of polarities in agreement with the solution and total polarity number.

N	Date	Time	M_D	Az1	Dip1	Rake1	Az2	Dip2	Rake2	FPS	Np	Sc
1	98-04-12	10:55:33.0	5.6	42	87	11	312	79	177	SS	71	0.95
2	98-04-12	13:35:27.5	3.7	176	51	-10	272	82	-140	SS	28	0.78
3	98-04-12	16:15:39.6	3.5	225	82	-5	315	84	-172	SS	34	0.76
4	98-04-12	22:13:48.3	3.8	18	47	92	194	43	87	TF	36	0.75
5	98-04-13	03:23:27.1	3.2	68	69	52	314	42	148	TS	30	0.90
6	98-04-15	19:40:30.6	3.9	139	39	51	240	81	51	SS	32	0.78
7	98-04-15	22:42:10.1	3.7	195	43	-42	318	43	-42	NF	30	0.76
8	98-04-16	17:21:44.3	3.4	23	38	-151	270	72	-55	NS	27	0.88
9	98-04-16	20:50:54.1	3.1	127	87	145	219	55	3	SS	18	0.77
10	98-04-18	10:15:40.5	3.2	59	12	-129	278	80	-82	NF	25	0.80
11	98-04-21	10:50:38.1	3.3	168	52	-87	343	38	-93	NF	31	0.83
12	98-04-22	06:56:28.9	3.7	176	51	-89	354	39	-91	NF	33	0.81
13	98-05-04	10:40:36.1	3.2	78	11	-129	298	81	-83	NF	18	0.77
14	98-05-06	02:53:00.4	4.6	106	62	117	239	38	50	TF	62	0.90
15	98-05-08	10:11:12.9	3.2	21	45	-78	184	46	-102	NF	29	0.79
16	98-05-11	23:30:49.0	3.7	121	76	131	226	42	20	TS	23	0.82
17	98-05-13	01:58:53.7	3.5	241	74	-44	346	47	-158	NS	29	0.89
18	98-05-13	21:37:39.7	3.2	141	80	-94	344	10	-67	NF	23	0.78
19	98-05-15	13:37:48.1	3.5	132	79	-98	350	14	-53	NF	30	0.86
20	98-05-24	17:45:24.0	3.1	121	29	-64	271	63	-104	NF	25	0.76
21	98-05-28	12:31:53.2	3.3	80	65	67	305	33	130	TF	17	0.76
22	98-06-10	23:32:41.3	3.2	178	32	-74	340	58	-99	NF	33	0.78
23	98-06-13	18:40:17.3	3.1	138	51	-99	332	39	-78	NF	22	0.81
24	98-06-17	18:10:09.0	3.0	92	47	113	239	47	66	TF	20	0.80
25	98-08-30	01:18:22.6	3.8	136	59	122	264	43	48	TF	25	0.80

Tab.1b

Focal parameters of the K98 Kobarid sequence. N: sequential number as in Table 4. other symbols are as in Table 1a.

N	Date	Time	M_D	Az1	Dip1	Rake1	Az2	Dip2	Rake2	FPS	Np	Sc
1	02-02-14	03:13:38.8	2.5	61	54	70	273	40	114	TF	18	0.88
2	02-02-14	03:18:03.2	4.9	63	54	67	278	41	118	TF	59	0.83
5	02-02-14	04:45:37.8	2.7	86	32	41	320	69	116	TF	25	0.92
6	02-02-17	14:37:18.2	2.2	143	18	-67	299	73	-97	NF	19	0.89
7	02-02-22	09:04:59.1	3.0	74	64	89	255	26	91	TF	31	0.83
8	02-02-25	10:55:23.0	3.2	86	32	66	294	60	104	TF	34	0.91
9	02-04-20	23:54:09.3	2.8	158	50	124	291	51	56	TF	27	0.81

Tab.1c

Focal parameters of the S02 Sernio sequence. N: sequential number as in Table 5. other symbols are as in Table 1a.

Event	Date	Time	M_D	Az1	Dip1	Rake1	Az2	Dip2	Rake2	FPS	Np	Sc
T98	98-05-28	09:32:19.4	4.1	82	79	90	258	11	84	TF	41	0.87
K04	04-07-12	13:04:06.4	5.1	305	79	-157	211	68	-11	SS	68	0.92

Tab.1d

Focal parameters of the May, 28 1998 Trasaghis earthquake (T98) and the July,12 2004 Kobarid earthquake (K04). Symbols are as in Table 1a.

Sequence	N	M_{Dc}	K	C	P	Std dev
C96 - 1	17	1.6	1.00	1.21	0.8	1.09
C96 – 2	30	1.7	3.69	0.13	1.0	1.09
C96 - 3	43	1.6	2.82	0.01	0.9	0.81
K98	557	2.0	31.70	0.51	0.8	6.43
S02	39	1.5	1.36	2.26	0.8	1.58

Tab. 2

Parameters of the Utsu's (1961) modified Omori law. N is the number of events, M_{Dc} is the duration magnitude completeness. K, C, P are the parameters of the regression, Std dev is the standard deviation. C96 -1, C96 – 2, C96 – 3 are the 3 sub-sequences that compose the C96 swarm

N	Date yy:mm:dd	Time hh:mm	ZONE	M_D	h(Zou) (km)	h(Bad) (km)	FPS	f_C (Hz)	M_0 (Nm)	$\Delta\sigma_B$ (MPa)	E_S (J)	σ_a (MPa)	$\Delta\sigma_{rms}$ (MPa)	r_B (m)	ϵ
1	96 01 27	08:26	Claut	3.5	43.3	54.4	TF	2.8	1.7e+14	0.89	2.3e+09	0.41	3.41	437	1.0
2	96 01 27	08:30	Claut	2.9	42.6	54.8	SS	4.6	1.7e+13	0.40	8.5e+07	0.14	0.84	267	1.1
3	96 01 27	15:28	Claut	2.9	42.6	53.9	NF	3.0	1.0e+13	0.07	8.1e+06	0.02	0.12	403	1.1
4	96 02 27	11:13	Claut	3.8	43.9	55.1	TF	2.1	7.8e+14	1.68	1.9e+10	0.70	5.65	589	1.1
5	96 02 27	11:26	Claut	2.6	43.5	54.7		4.0	3.6e+12	0.05	2.7e+06	0.02	0.11	307	1.1
6	96 02 27	11:37	Claut	2.7	42.8	54.6		4.6	3.1e+12	0.07	2.9e+06	0.03	0.15	267	1.1
7	96 02 27	12:38	Claut	2.8	43.6	55.1	TF	5.4	2.0e+13	0.75	2.3e+08	0.33	1.37	228	1.0
8	96 02 27	13:43	Claut	3.1	43.2	55.0	NF	4.6	6.1e+13	1.39	1.2e+09	0.56	3.06	268	1.1
9	96 02 27	19:47	Claut	2.5	41.5	53.6	NF	4.8	5.7e+12	0.14	9.5e+06	0.05	0.32	258	1.1
10	96 02 28	13:02	Claut	2.5	42.5	54.2		6.0	2.1e+12	0.11	2.7e+06	0.04	0.22	204	1.1
11	96 03 05	05:56	Claut	2.4	43.3	54.7		7.1	3.2e+12	0.26	1.2e+07	0.11	0.61	174	1.0
12	96 04 13	02:01	Claut	3.0	42.8	53.9		5.8	5.5e+12	0.26	1.7e+07	0.09	0.47	211	1.1
13	96 04 13	13:00	Claut	4.3	43.6	54.6	TF	2.0	1.2e+15	2.30	4.3e+10	1.06	7.65	612	1.0
14	96 04 13	13:09	Claut	2.3	42.5	53.7		4.4	3.7e+12	0.07	3.3e+06	0.03	0.28	280	1.1
15	96 04 14	07:29	Claut	2.7	42.9	54.3		3.9	4.4e+12	0.06	3.6e+06	0.02	0.12	312	1.1
16	96 04 15	13:07	Claut	2.9	43.2	54.0	NS	4.8	4.0e+13	1.04	5.4e+08	0.40	2.26	257	1.1
17	96 04 16	18:06	Claut	3.5	42.5	54.4	SS	3.4	1.6e+14	1.53	3.1e+09	0.58	3.50	356	1.1
18	96 05 06	10:20	Clautana	2.9	42.7	53.4	NF	5.1	1.9e+13	0.59	1.7e+08	0.26	1.35	243	1.0
19	96 05 11	07:39	Claut	2.5	41.8	53.0		4.1	3.0e+12	0.05	1.6e+06	0.02	0.11	300	1.1
20	96 06 01	19:49	Claut	2.3	43.8	54.8		4.8	1.7e+12	0.05	9.4e+05	0.02	0.10	254	1.1
m				2.3	41.5	53.0		2.0	1.7e+12	0.05	9.4e+05	0.02	0.10	174	1.0
M				4.3	43.9	55.1		7.1	1.2e+15	2.30	4.3e+10	1.06	7.65	612	1.1
Av										0.59		0.24	1.58		
E								1.2	1.3	1.7	3.1	3.2	3.3	1.2	3.6

Tab.3

Tab.3 – 1996 Claut swarm (C96): source parameters of the analyzed events. M_D : duration magnitude; h(Zou): hypocentral distance from station ZOU; h(Bad): hypocentral distance from station BAD; FPS: fault plane solution according to Zoback (1992); f_C : corner frequency; M_0 : seismic moment; $\Delta\sigma_B$: Brune stress drop; E_S : radiated energy; σ_a: apparent stress; $\Delta\sigma_{rms}$: RMS stress drop; r_B: Brune radius; ϵ: Zuniga parameter. “m” and “M” stands for minimum and maximum values of each parameter, respectively. Av: average value. “E” is the mean multiplicative error of the lognormal distribution of each parameter.

N	Date yy:mm:dd	Time hh:mm	ZONE	M_D	h(Zou) (km)	h(Bad) (km)	FPS	f_C (Hz)	M_0 (Nm)	$\Delta\sigma_B$ (MPa)	E_S (J)	σ_a (MPa)	$\Delta\sigma_{rms}$ (MPa)	r_B (m)	ϵ
1	98 04 12	10:55	Kobarid	5.6	59.1	33.0	SS	0.5	1.1e+17	2.62	9.9e+12	2.55	6.38	2672	0.7
2	98 04 12	13:35	Zaga	3.7	57.7	27.9	SS	3.2	1.4e+14	1.09	1.2e+09	0.24	4.28	388	1.4
3	98 04 12	16:15	Kobarid	3.5	56.6	30.3	SS	3.1	9.8e+13	0.66	1.0e+09	0.30	0.36	402	1.0
4	98 04 12	22:13	Kobarid	3.8	56.9	30.7	TF	2.5	1.7e+14	0.61	3.0e+09	0.52	1.44	496	0.7
5	98 04 13	03:23	Kobarid	3.2	56.9	30.8	TS	4.1	5.5e+13	1.01	7.0e+08	0.39	1.65	302	1.1
6	98 04 15	19:40	Kuk	3.9	66.8	37.9	SS	1.8	3.1e+14	0.43	2.4e+09	0.23	0.51	679	1.0
7	98 04 15	22:42	Kobarid	3.7	59.7	33.6	NF	1.4	4.6e+14	0.31	1.1e+09	0.07	0.21	865	1.4
8	98 04 16	17:21	Kobarid	3.4	61.6	33.6	NS	3.8	3.7e+13	0.49	3.9e+08	0.31	0.88	320	0.9
9	98 04 16	20:50	Kobarid	3.1	59.3	32.8	SS	2.5	2.8e+13	0.07	2.4e+07	0.04	0.12	494	0.9
10	98 04 18	10:15	kobarid	3.2	63.0	36.4	NF	2.6	4.9e+13	0.19	2.1e+08	0.17	0.40	473	0.7
11	98 04 21	10:50	Kobarid	3.3	55.0	29.9	NF	3.1	5.8e+13	0.41	3.2e+08	0.17	0.70	395	1.1
12	98 04 22	06:56	Kobarid	3.7	64.1	34.9	NF	2.7	9.5e+13	0.42	8.3e+08	0.26	0.80	462	0.9
13	98 05 04	10:40	Kobarid	3.2	64.1	35.5	NF	4.9	2.1e+13	0.60	1.6e+08	0.26	1.13	252	1.1
14	98 05 06	02:53	Kobarid	4.6	63.9	35.3	TF	1.5	2.0e+15	1.49	9.5e+10	1.41	3.19	836	0.7
15	98 05 08	10:11	Kobarid	3.2	64.5	36.1	NF	4.4	3.6e+13	0.84	7.1e+08	0.55	1.11	282	0.9
16	98 05 11	23:30	Kuk	3.7	64.1	36.1	TS	2.1	2.6e+14	0.55	1.9e+09	0.22	1.42	591	1.1
17	98 05 13	01:58	Kuk	3.5	64.3	36.1	NS	2.9	8.0e+13	0.46	8.2e+08	0.30	1.03	424	0.9
18	98 05 13	21:37	Kuk	3.2	67.9	39.7	NF	3.5	2.2e+13	0.24	1.2e+08	0.16	0.37	349	0.8
19	98 05 15	13:37	Kobarid	3.5	58.3	31.4	NF	4.9	3.5e+13	0.98	9.2e+08	0.77	1.81	251	0.8
20	98 05 24	17:45	Kobarid	3.1	63.6	36.1	NF	5.2	2.7e+13	1.02	3.5e+08	0.37	1.71	237	1.1
21	98 05 28	12:31	Kuk	3.3	65.3	37.1	TF	4.2	3.4e+13	0.66	5.2e+08	0.44	1.13	293	0.8
22	98 06 10	23:32	Kobarid	3.2	59.0	32.9	NF	4.3	9.5e+13	2.31	5.8e+09	1.62	4.79	286	0.8
23	98 06 13	18:40	Kobarid	3.1	64.3	36.3	NF	7.0	4.4e+13	1.93	2.0e+09	0.76	5.86	175	1.1
24	98 06 17	18:10	Kobarid	3.0	60.1	32.8	TF	2.9	2.9e+13	0.18	1.0e+08	0.11	0.32	421	0.9
25	98 08 30	01:18	Drenchia	3.8	65.6	34.5	TF	1.7	1.9e+14	0.24	1.7e+09	0.26	0.64	706	0.6
m				3.0	55.0	27.9		0.5	2.1e+13	0.07	2.4e+07	0.04	0.12	175	0.6
M				5.6	65.6	39.7		7.0	1.1e+17	2.62	9.9e+12	2.55	6.38	2672	1.4
Av										0.79		0.50	1.69		
E								1.2	1.4	2.1	3.7	3.9	4.3	1.2	4.8

Tab. 4

Tab.4 – 1998 Kobarid sequence (K98): source parameters of the analyzed events. Symbols are as in Tab. 3.

N	Date yy:mm:dd	Time hh:mm	ZONE	M_D	h(Zou) (km)	h(Bad) (km)	FPS	f_C (Hz)	M_0 (Nm)	$\Delta\sigma_B$ (MPa)	E_S (J)	σ_a (MPa)	$\Delta\sigma_{rms}$ (MPa)	r_B (m)	Є
1	02 02 14	03:13	M.Sernio	2.5	21.9	27.7	TF	6.2	3.6e+12	0.20	1.2e+07	0.10	0.27	199	1.0
2	02 02 14	03:18	M.Sernio	4.9	21.1	28.5	TF	1.4	8.4e+15	5.31	9.2e+11	3.23	12.69	884	0.9
3	02 02 14	03:26	M.Sernio	2.3	22.1	27.5		5.0	1.1e+13	0.59	4.9e+07	0.11	0.56	201	1.4
4	02 02 14	03:36	M.Sernio	2.2	22.0	26.7		7.8	4.0e+12	0.82	2.4e+07	0.14	0.75	128	1.5
5	02 02 14	04:45	M.Sernio	2.7	21.7	26.6	TF	6.9	7.3e+12	0.27	3.8e+07	0.22	2.00	177	0.7
6	02 02 17	14:37	Arta	2.2	19.9	28.0	NF	7.7	2.3e+12	0.24	5.0e+06	0.36	0.85	160	0.5
7	02 02 22	09:04	Tolmezzo	3.0	25.3	18.6	TF	2.7	2.9e+13	0.15	5.3e+07	0.05	0.52	453	1.2
8	02 02 25	10 :55	M.Sernio	3.2	21.3	26.5	TF	5.2	3.0e+13	1.87	4.6e+08	0.36	1.96	191	1.4
9	02 04 20	23:54	M.Sernio	2.8	19.6	26.0	TF	5.0	1.1e+13	0.38	1.3e+08	0.28	0.69	246	0.8
10	02 06 30	19:16	M.Sernio	2.3	17.6	30.5		5.6	4.1e+12	0.31	9.6e+06	0.06	0.28	180	1.4
m				2.2	17.6	18.6		1.4	2.3e+12	0.15	5.0e+06	0.05	0.27	128	0.5
M				4.9	25.3	30.5		7.8	8.4e+15	5.31	9.2e+11	3.23	12.69	884	1.5
Av										1.0		0.49	2.0		
E								1.3	1.5	2.5	3.4	3.6	5.0	1.3	4.9

Tab.5

Tab.5 – 2002 M.te Sernio sequence (S02): source parameters of the analyzed events. Symbols are as in Tab. 3.

N	Date yy:mm:dd	Time hh:mm	ZONE	M_D	M_0 (Nm)	$\Delta\sigma_B$ (MPa)	σ_a (MPa)	$\Delta\sigma_{rms}$ (MPa)	r_B (m)	Є	R_{ES}
1	96 01 27	08:26	Claut	3.5	1.7e+14	0.89	0.41	3.41	437	1.0	11.1
2	96 02 27	11:13	Claut	3.8	7.8e+14	1.68	0.70	5.65	589	1.1	46.0
3	96 04 13	13:00	Claut	4.3	1.2e+15	2.30	1.06	7.65	612	1.0	31.7
4	98 04 12	10:55	Kobarid	5.6	1.1e+17	2.62	2.55	6.38	2672	0.7	51.0
5	98 05 28	09:32	Trasaghis	4.1	1.1e+14	3.00	2.20	8.40	252	0.8	54.7
6	02 02 14	03:18	M.Sernio	4.9	8.4e+15	5.31	3.23	12.69	884	0.9	1732.6
7	04 07 12	13:04	Kobarid	5.1	2.6e+16	3.65	3.00	9.50	1540	0.7	432.7
E					1.2	1.9	2.8	3.7	1.2	3.4	4.2

Tab. 6

Tab.6 - Source parameters of the mainshocks. R_{ES} is the ratio between the energy radiated by the mainshock and the summation of the energies radiated by the aftershocks. Other parameters are as in Tables 3,4 and 5.

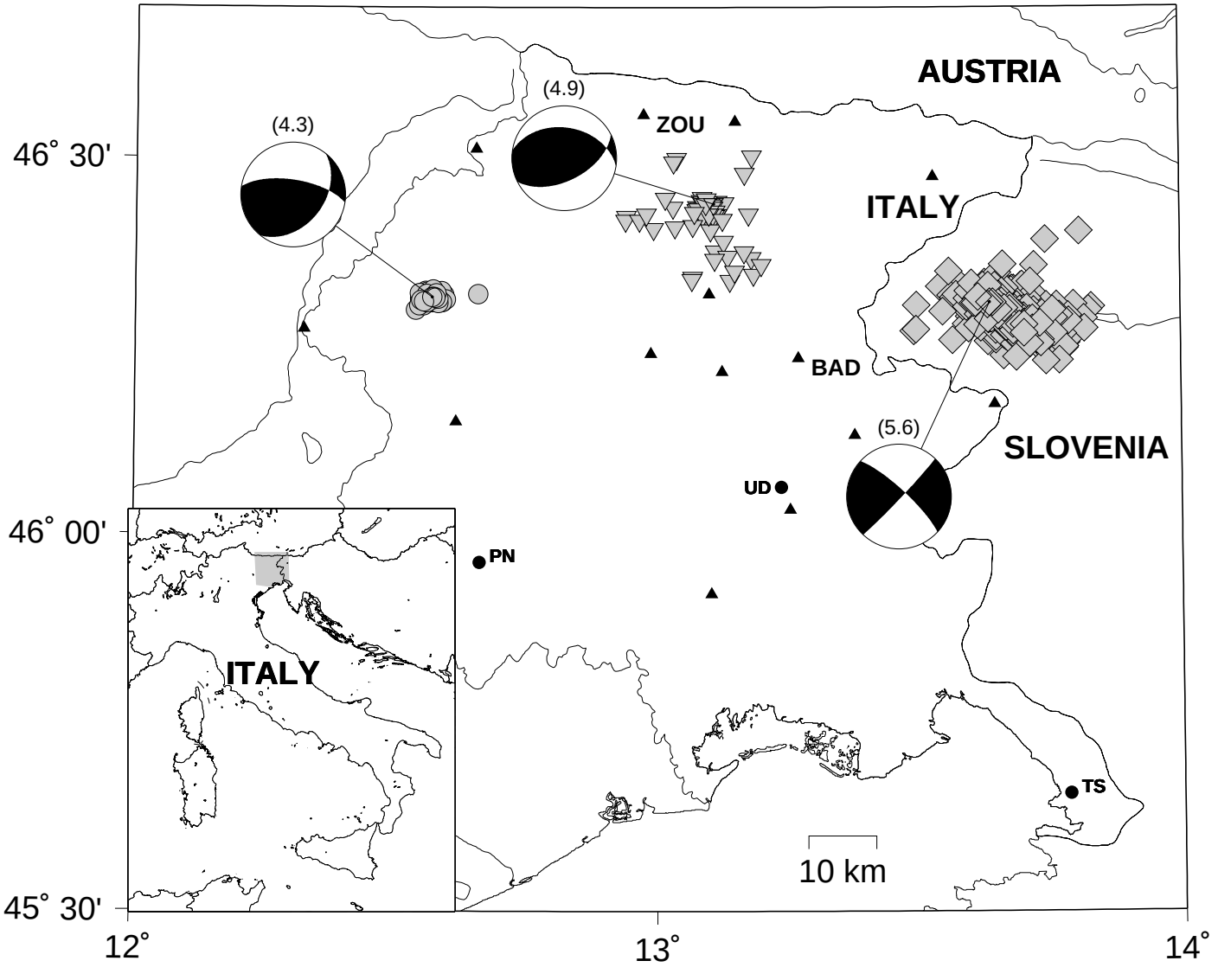
AUSTRIA
ITALY
SLOVENIA
(4.3)
(4.9)
(5.6)
ZOU
BAD
UD
PN
TS
ITALY
10 km
46° 30'
46° 00'
45° 30'
12°
13°
14°

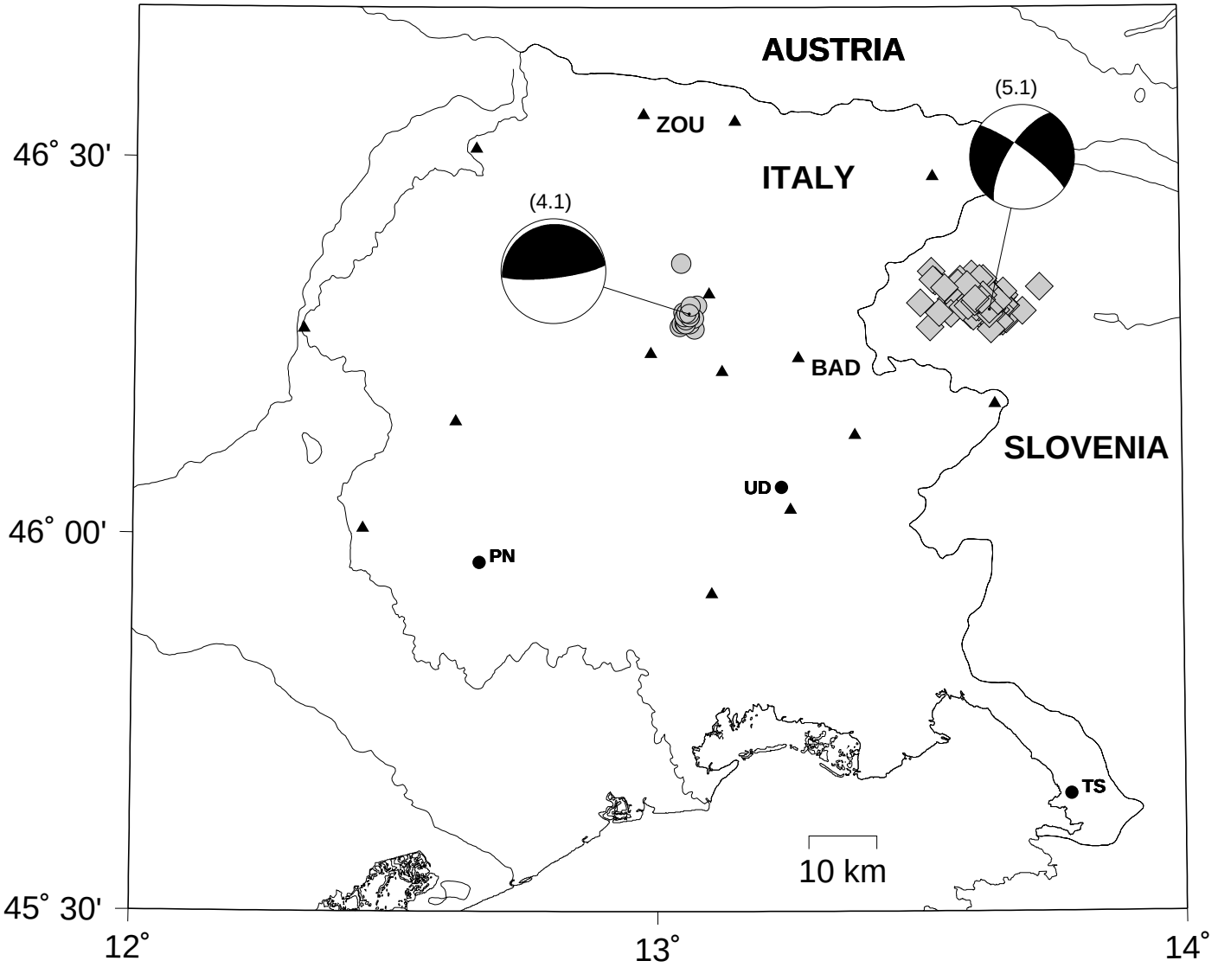
AUSTRIA
ITALY
SLOVENIA
ZOU
BAD
UD
PN
TS
(4.1)
(5.1)
10 km
46° 30'
46° 00'
45° 30'
12°
13°
14°

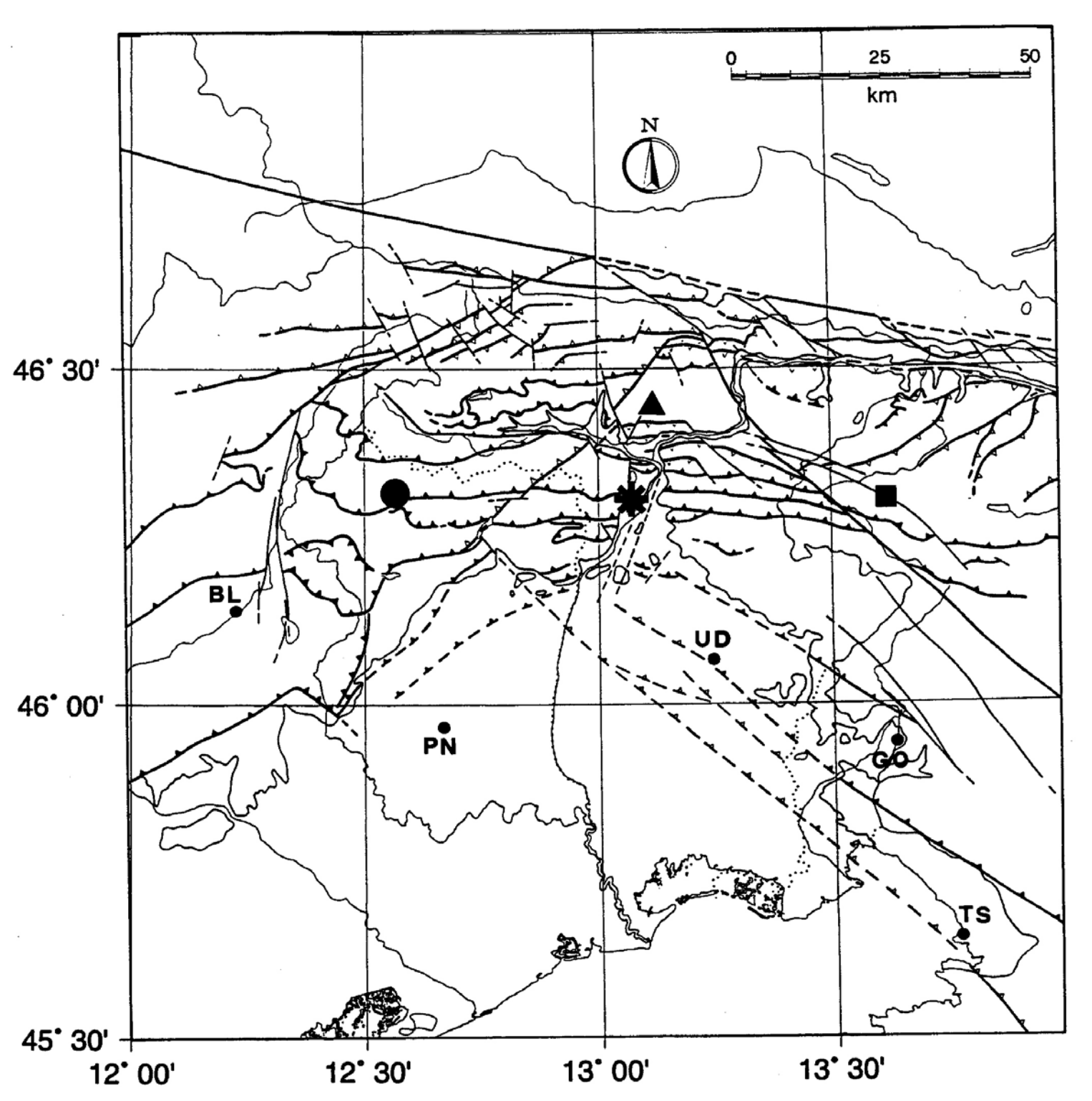
0
25
50
km
N
46° 30'
46° 00'
45° 30'
12° 00'
12° 30'
13° 00'
13° 30'
BL
UD
PN
GO
TS

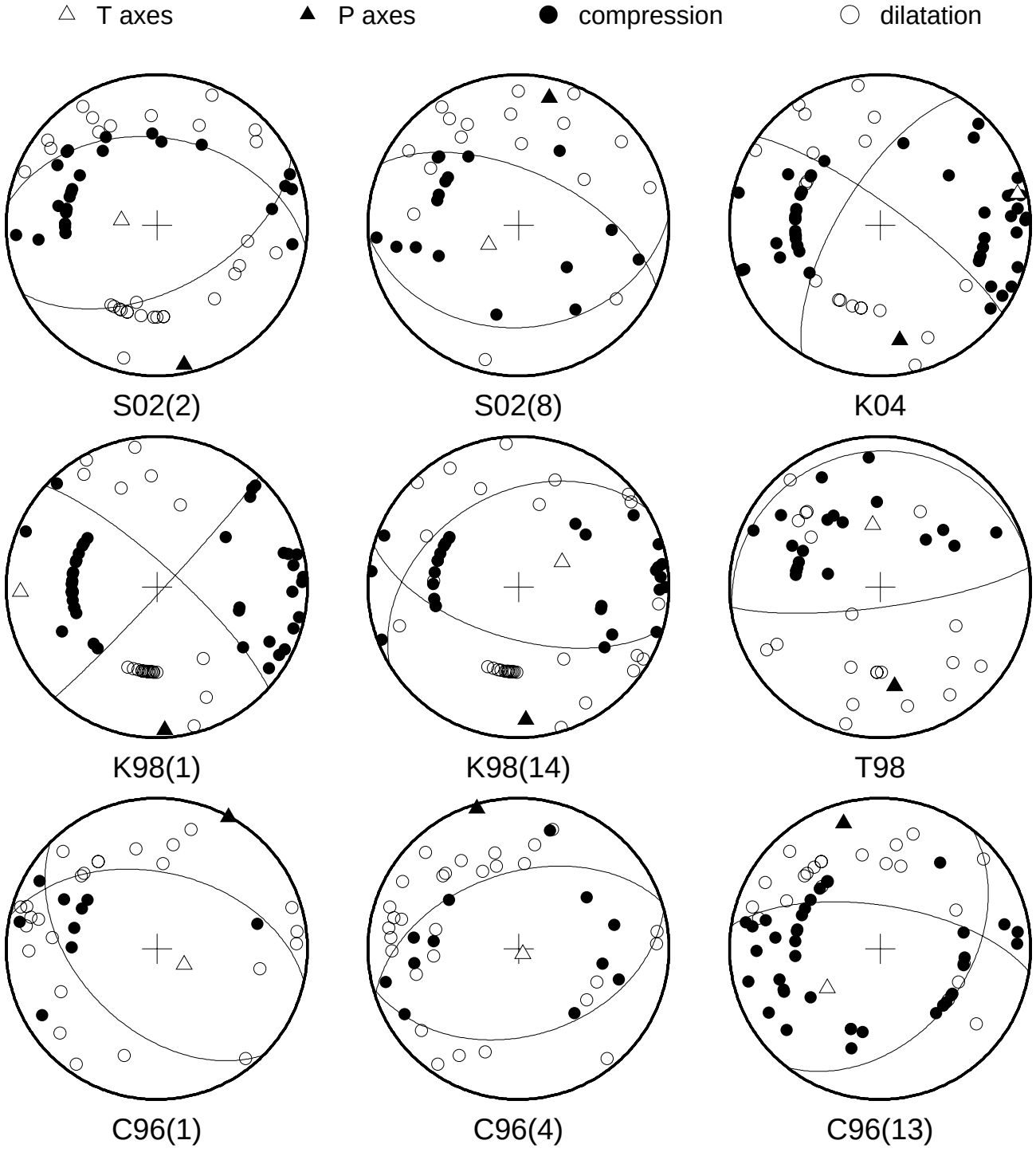
T axes
P axes
compression
dilatation
S02(2)
S02(8)
K04
K98(1)
K98(14)
T98
C96(1)
C96(4)
C96(13)

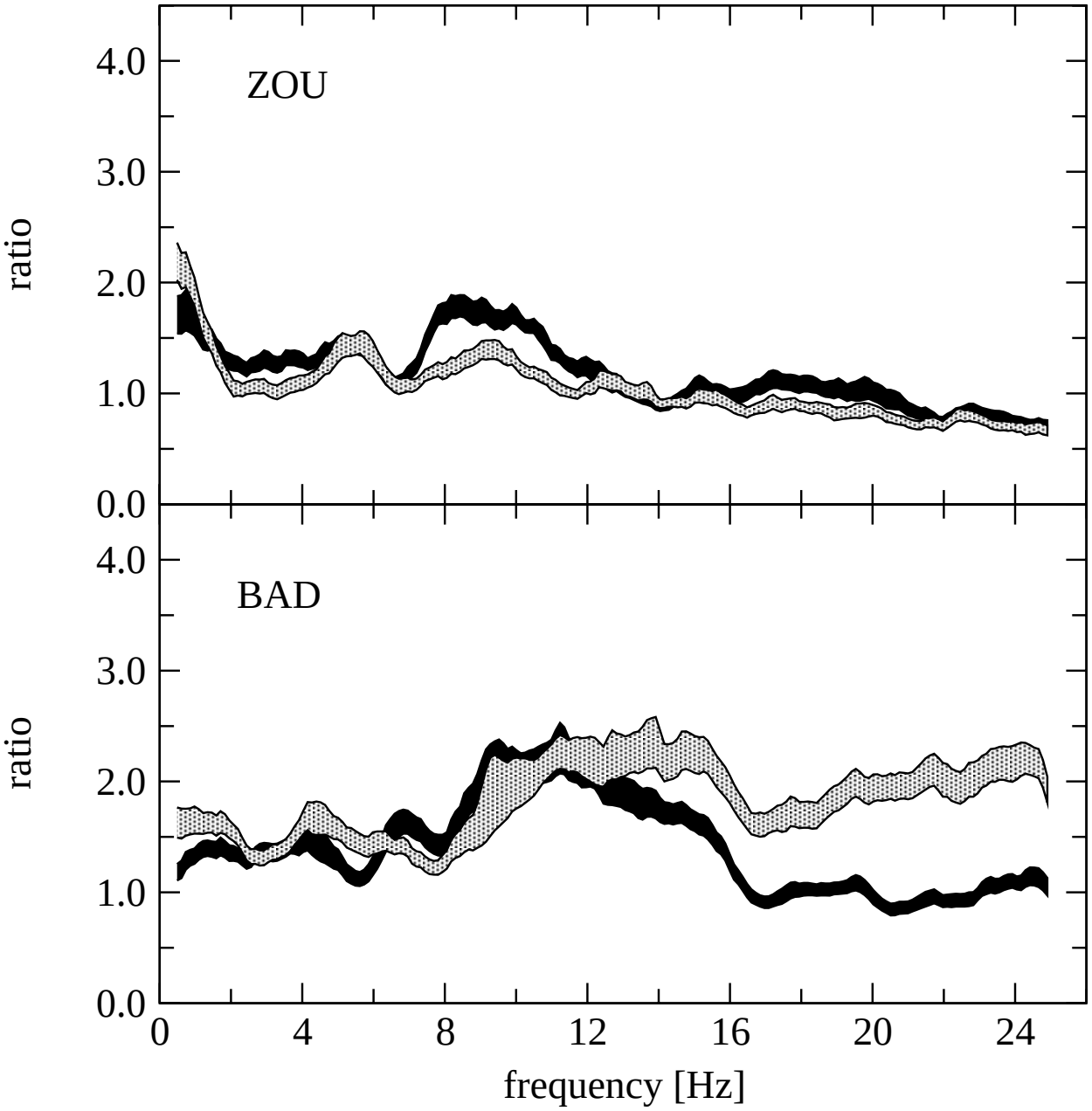
ZOU
BAD
ratio
ratio
4.0
3.0
2.0
1.0
0.0
0
4
8
12
16
20
24
frequency [Hz]

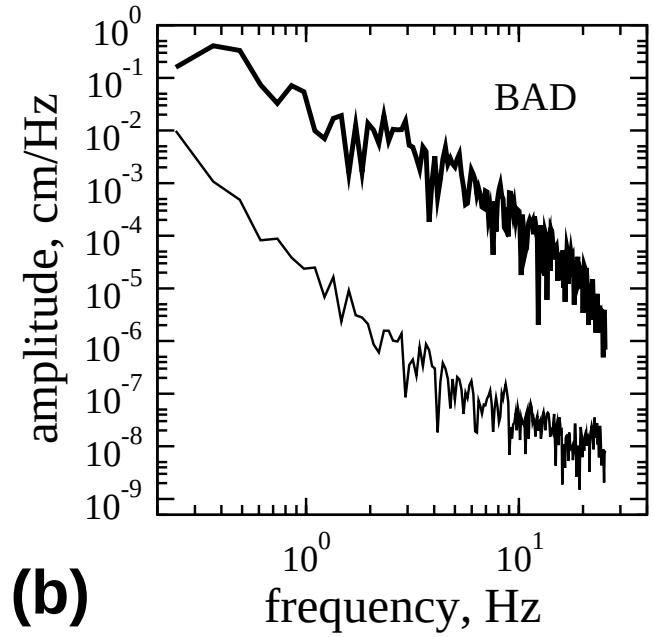
BAD
amplitude, cm/Hz
frequency, Hz

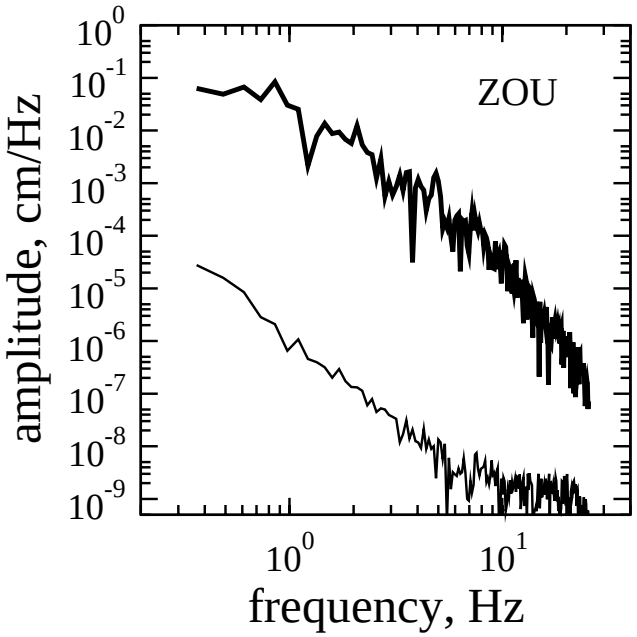
ZOU
amplitude, cm/Hz
frequency, Hz

(b)

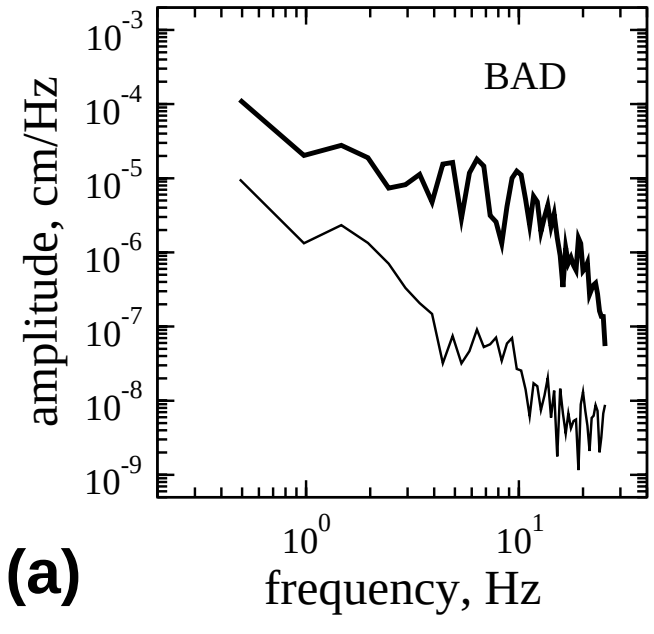
BAD
amplitude, cm/Hz
frequency, Hz

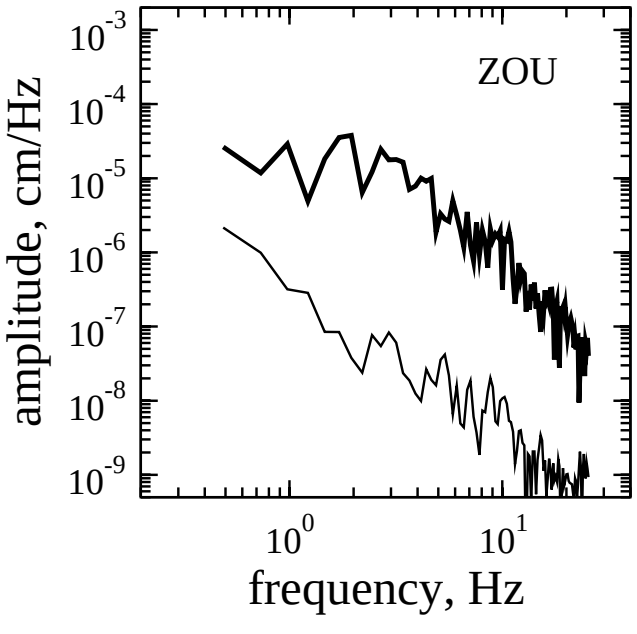
ZOU
amplitude, cm/Hz
frequency, Hz

(a)

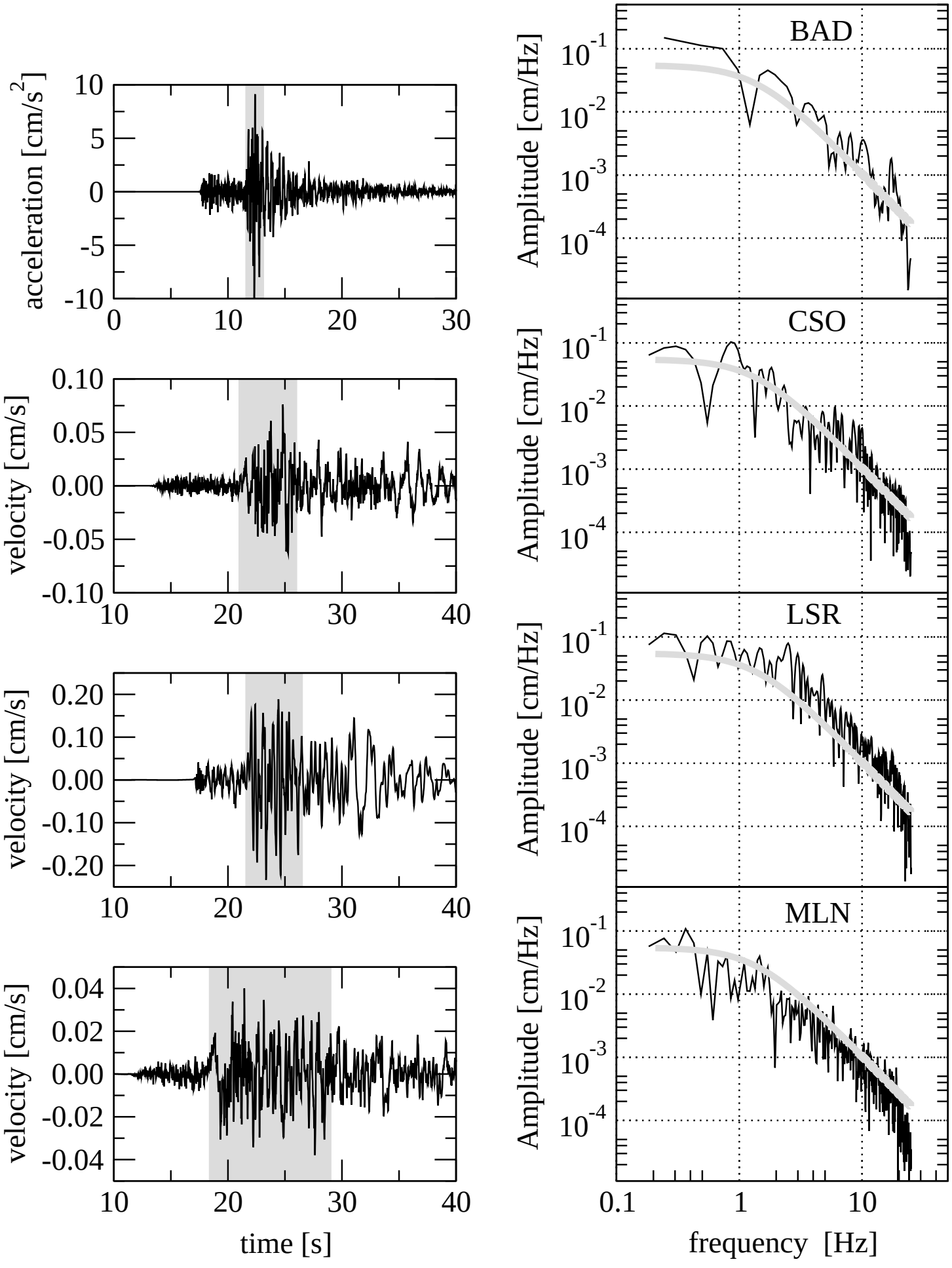
acceleration [cm/s^2]
velocity [cm/s]
velocity [cm/s]
velocity [cm/s]
time [s]
BAD
CSO
LSR
MLN
Amplitude [cm/Hz]
frequency [Hz]

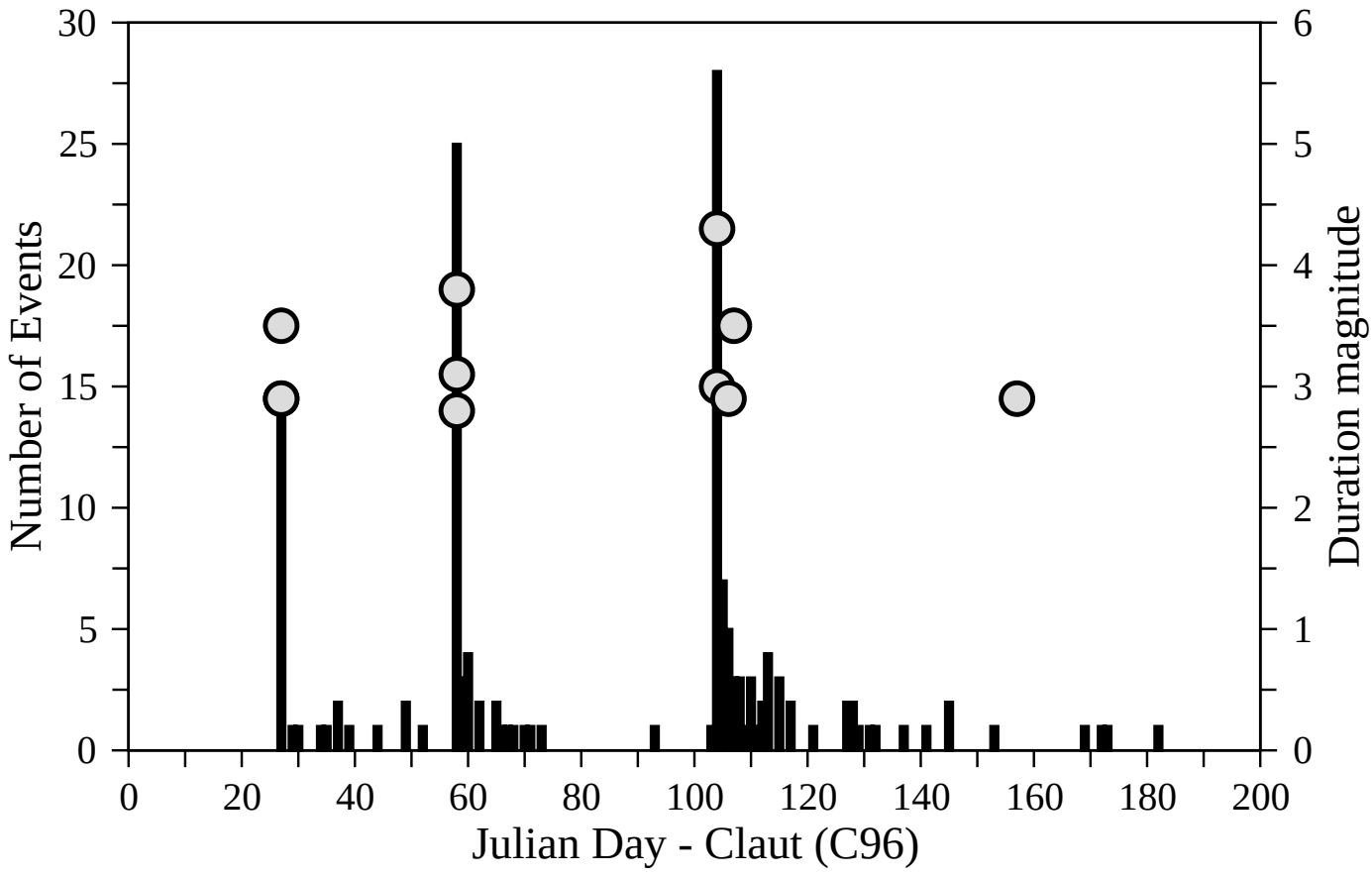
Number of Events
Duration magnitude
Julian Day - Claut (C96)
0
5
10
15
20
25
30
0
1
2
3
4
5
6
0
20
40
60
80
100
120
140
160
180
200

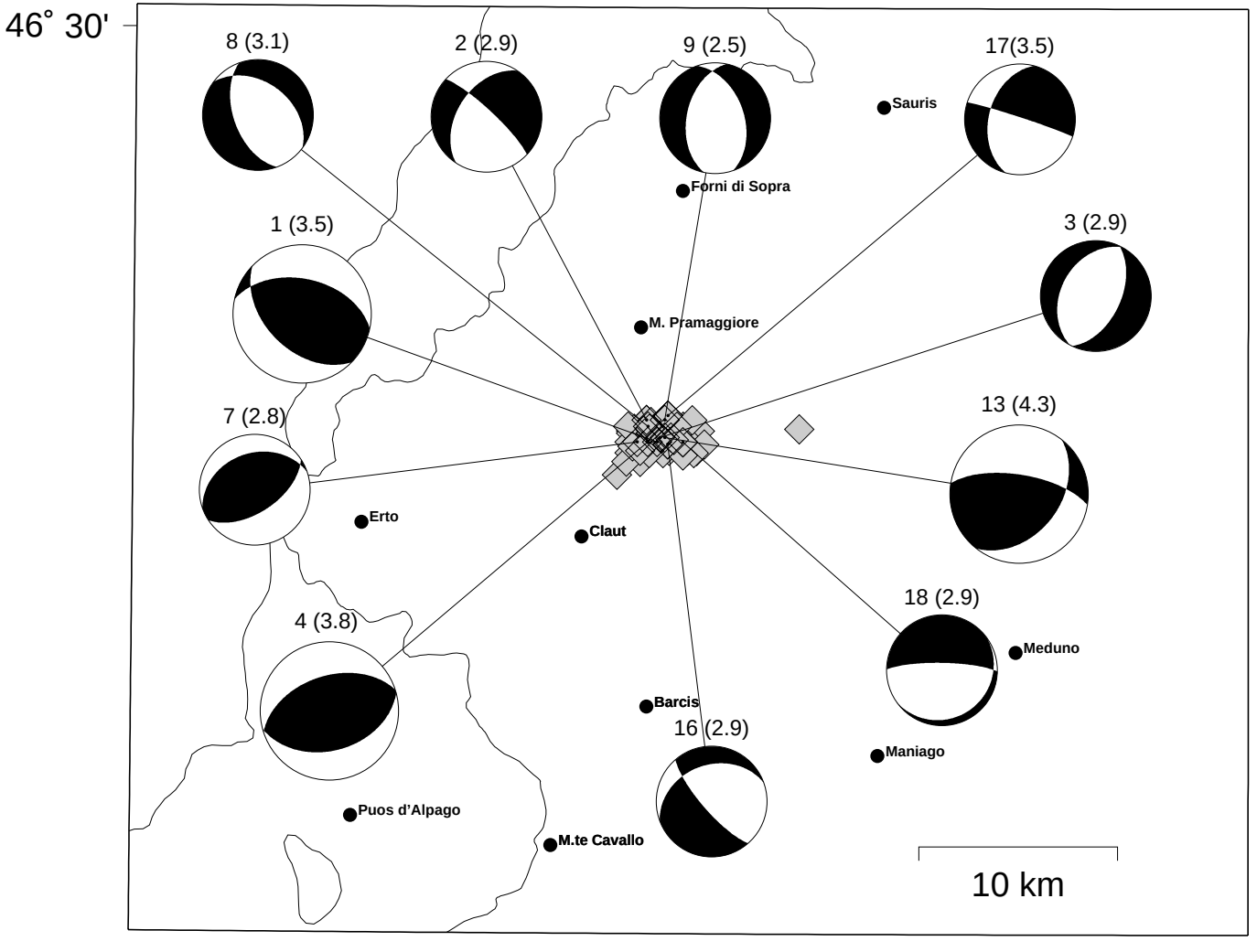
46° 30'
8 (3.1)
2 (2.9)
9 (2.5)
17(3.5)
Sauris
Forni di Sopra
1 (3.5)
3 (2.9)
M. Pramaggiore
7 (2.8)
13 (4.3)
Erto
Claut
18 (2.9)
4 (3.8)
Meduno
Barcis
16 (2.9)
Maniago
Puos d'Alpago
M.te Cavallo
10 km

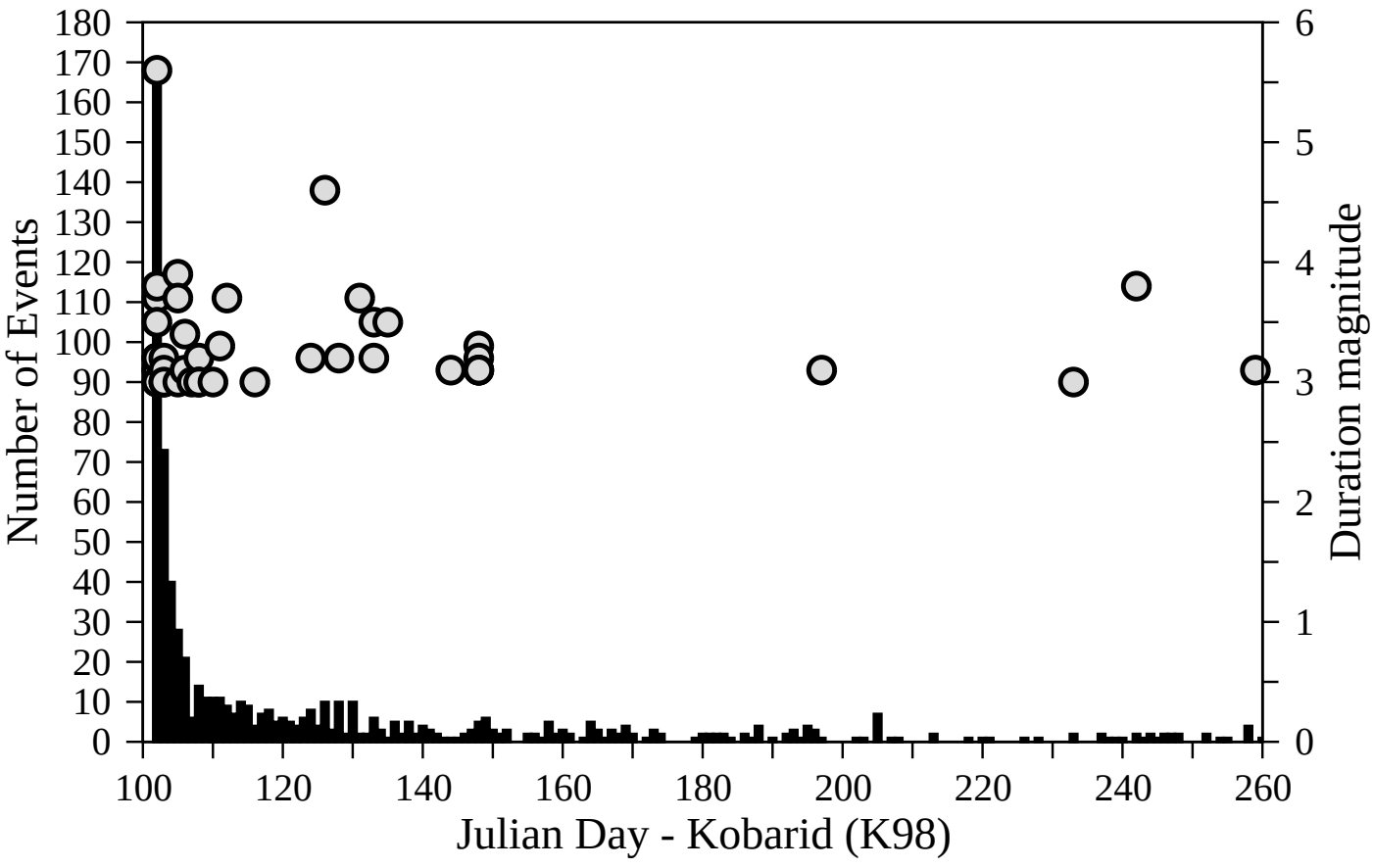
Number of Events
Duration magnitude
Julian Day - Kobarid (K98)
0
10
20
30
40
50
60
70
80
90
100
110
120
130
140
150
160
170
180
0
1
2
3
4
5
6
100
120
140
160
180
200
220
240
260

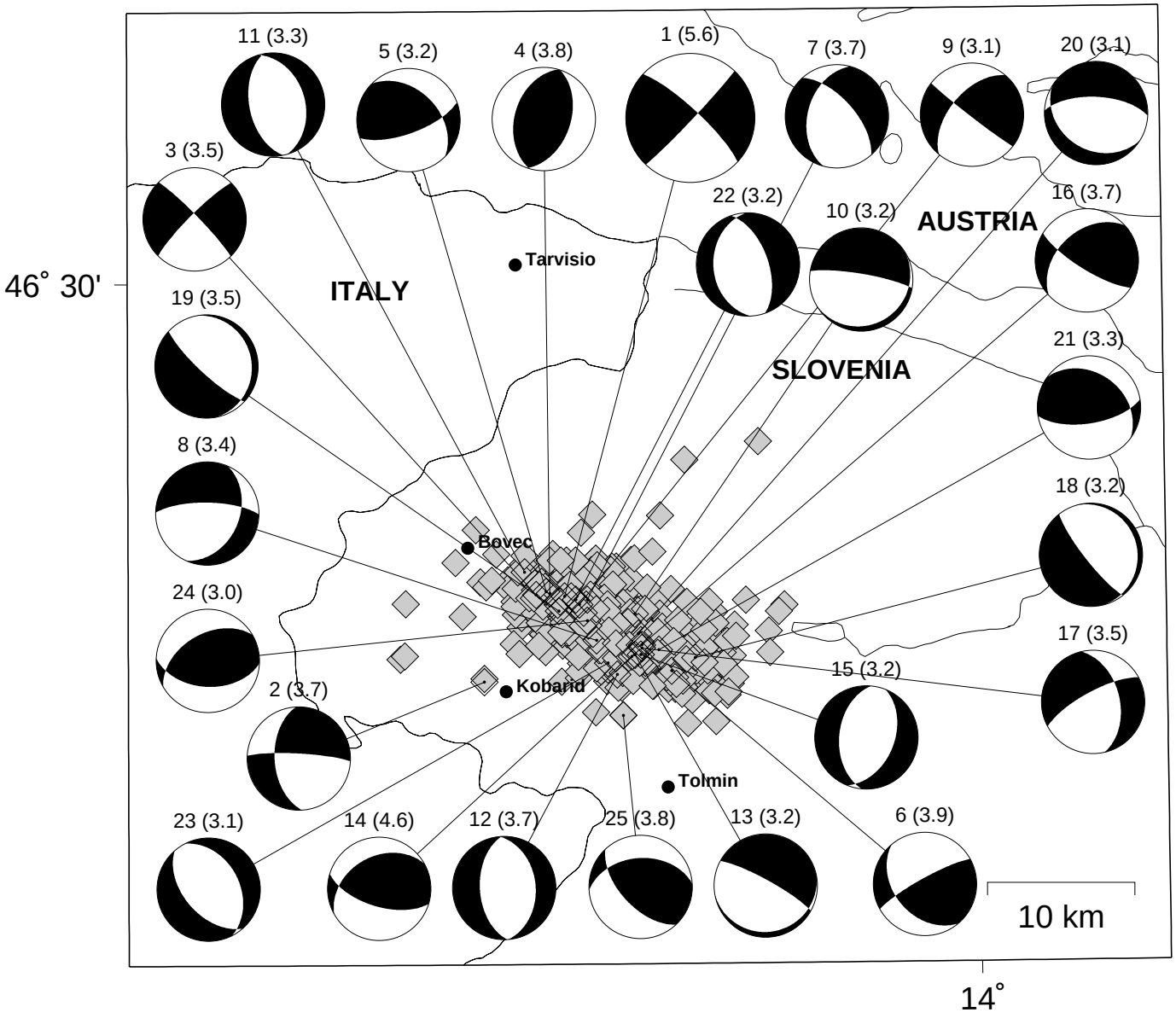
11 (3.3)
5 (3.2)
4 (3.8)
1 (5.6)
7 (3.7)
9 (3.1)
20 (3.1)
3 (3.5)
22 (3.2)
10 (3.2)
AUSTRIA
16 (3.7)
46° 30'
Tarvisio
ITALY
19 (3.5)
SLOVENIA
21 (3.3)
8 (3.4)
18 (3.2)
Bovec
24 (3.0)
17 (3.5)
15 (3.2)
2 (3.7)
Kobarid
Tolmin
23 (3.1)
14 (4.6)
12 (3.7)
25 (3.8)
13 (3.2)
6 (3.9)
10 km
14°

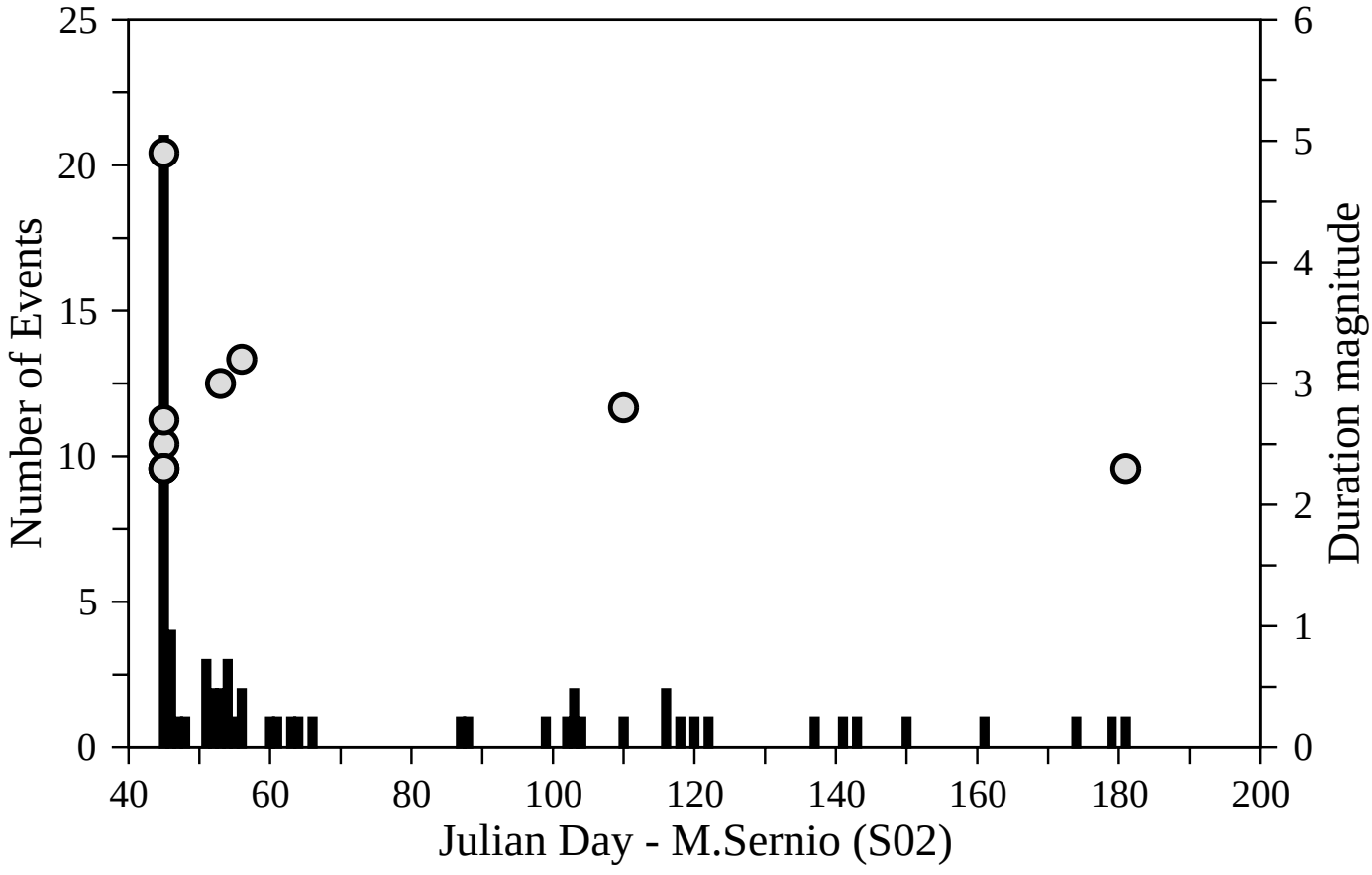
Number of Events
Duration magnitude
Julian Day - M.Sernio (S02)
0
5
10
15
20
25
0
1
2
3
4
5
6
40
60
80
100
120
140
160
180
200

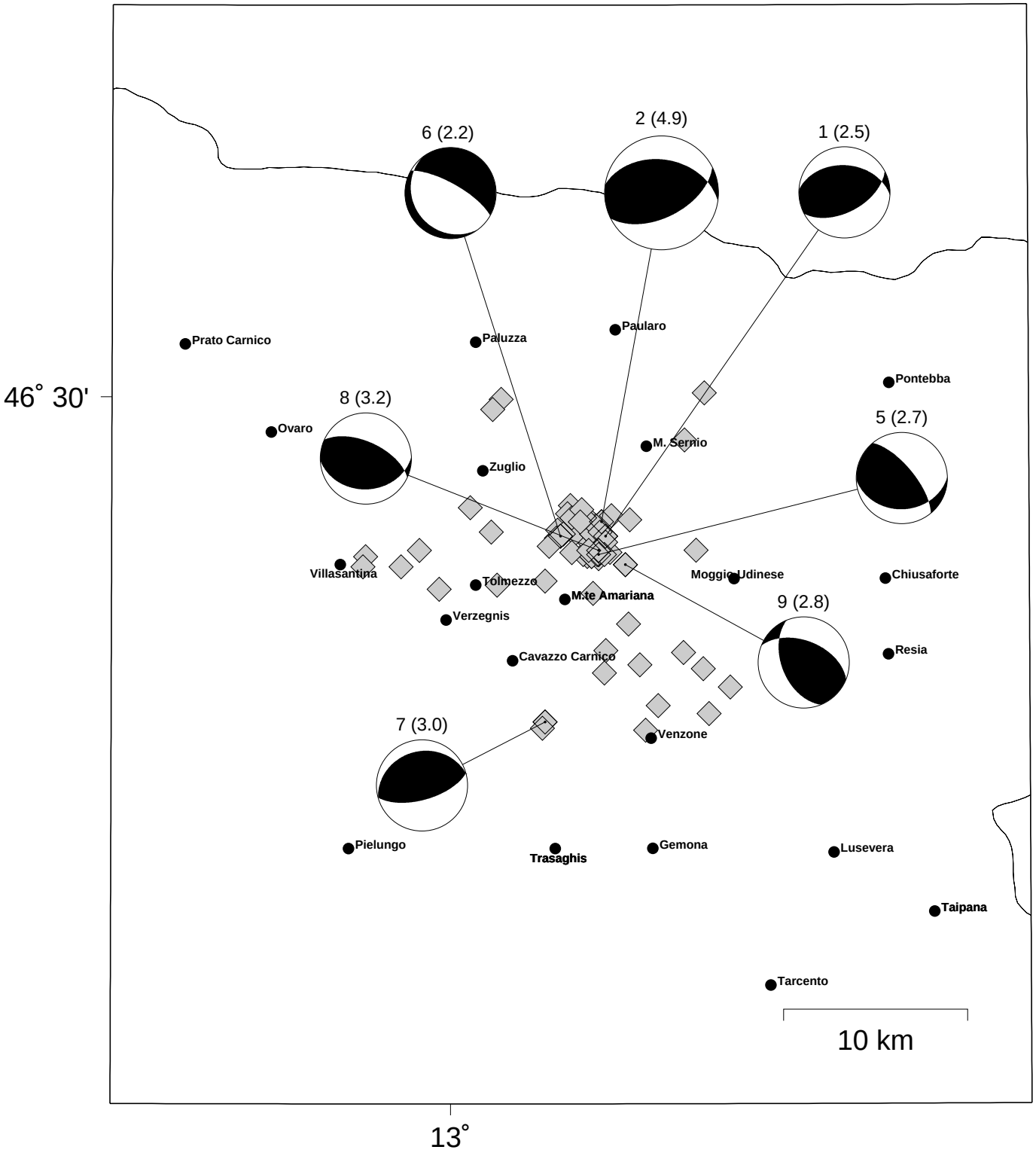
6 (2.2)
2 (4.9)
1 (2.5)
Prato Carnico
Paluzza
Paularo
46° 30'
Pontebba
8 (3.2)
Ovaro
5 (2.7)
M. Sernio
Zuglio
Villasantina
Tolmezzo
Moggio Udinese
Chiusaforte
M.te Amariana
9 (2.8)
Verzegnis
Resia
Cavazzo Carnico
7 (3.0)
Venzone
Pielungo
Trasaghis
Gemona
Lusevera
Taipana
Tarcento
10 km
13°

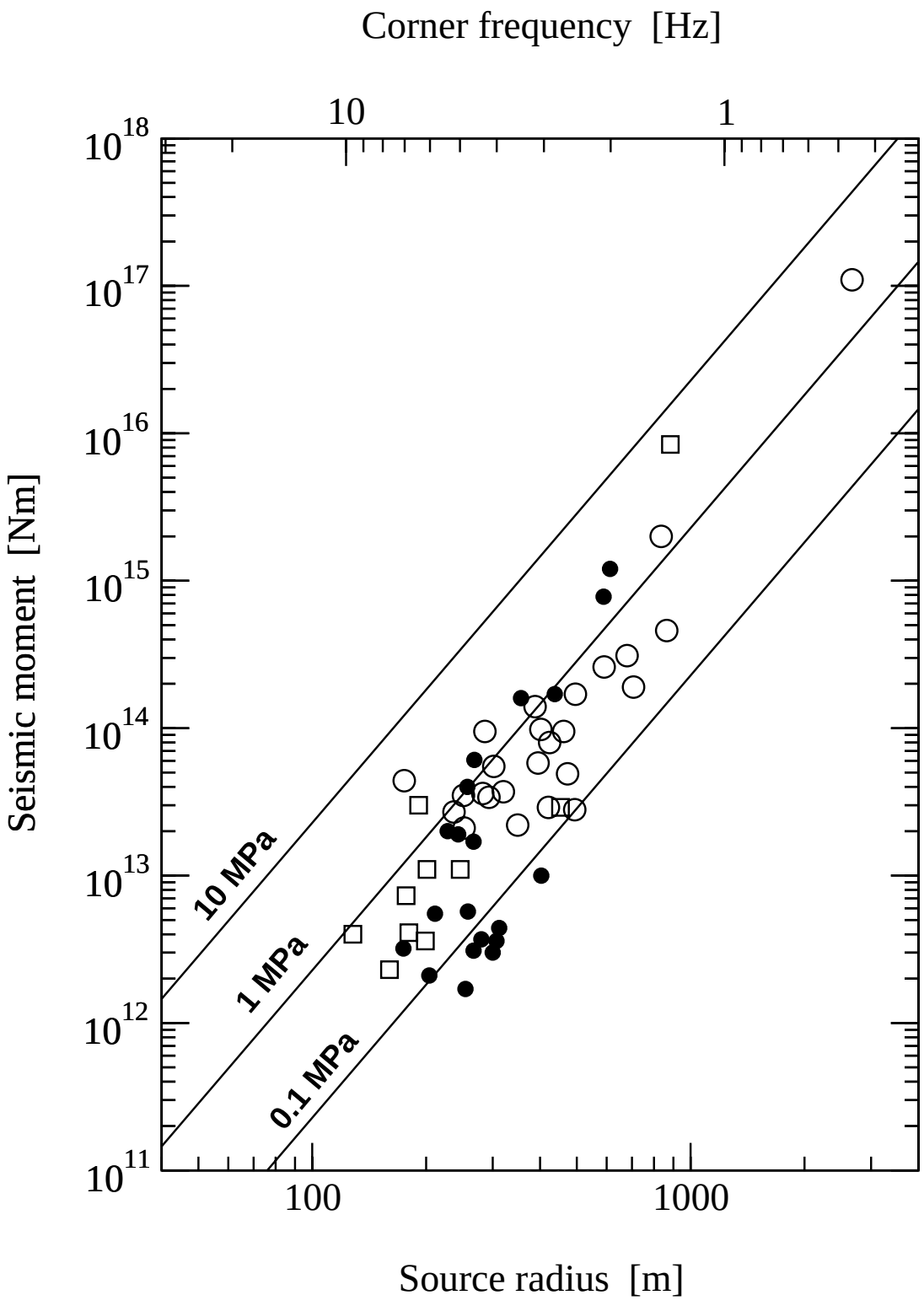
Corner frequency [Hz]
10
1
10^{18}
10^{17}
10^{16}
10^{15}
10^{14}
10^{13}
10^{12}
10^{11}
Seismic moment [Nm]
10 MPa
1 MPa
0.1 MPa
100
1000
Source radius [m]

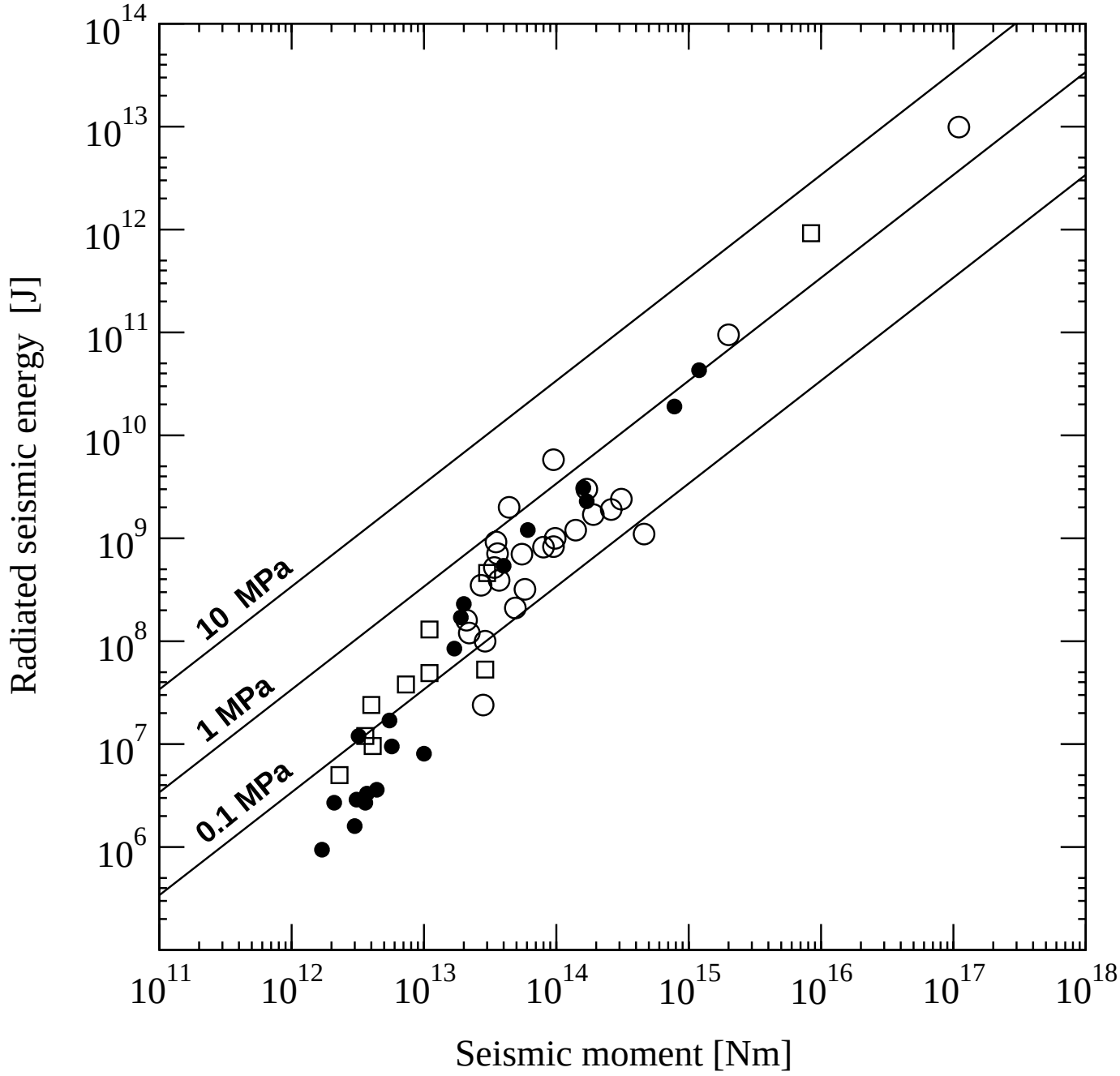
Radiated seismic energy [J]
Seismic moment [Nm]
10 MPa
1 MPa
0.1 MPa
10^14
10^13
10^12
10^11
10^10
10^9
10^8
10^7
10^6
10^11
10^12
10^13
10^14
10^15
10^16
10^17
10^18

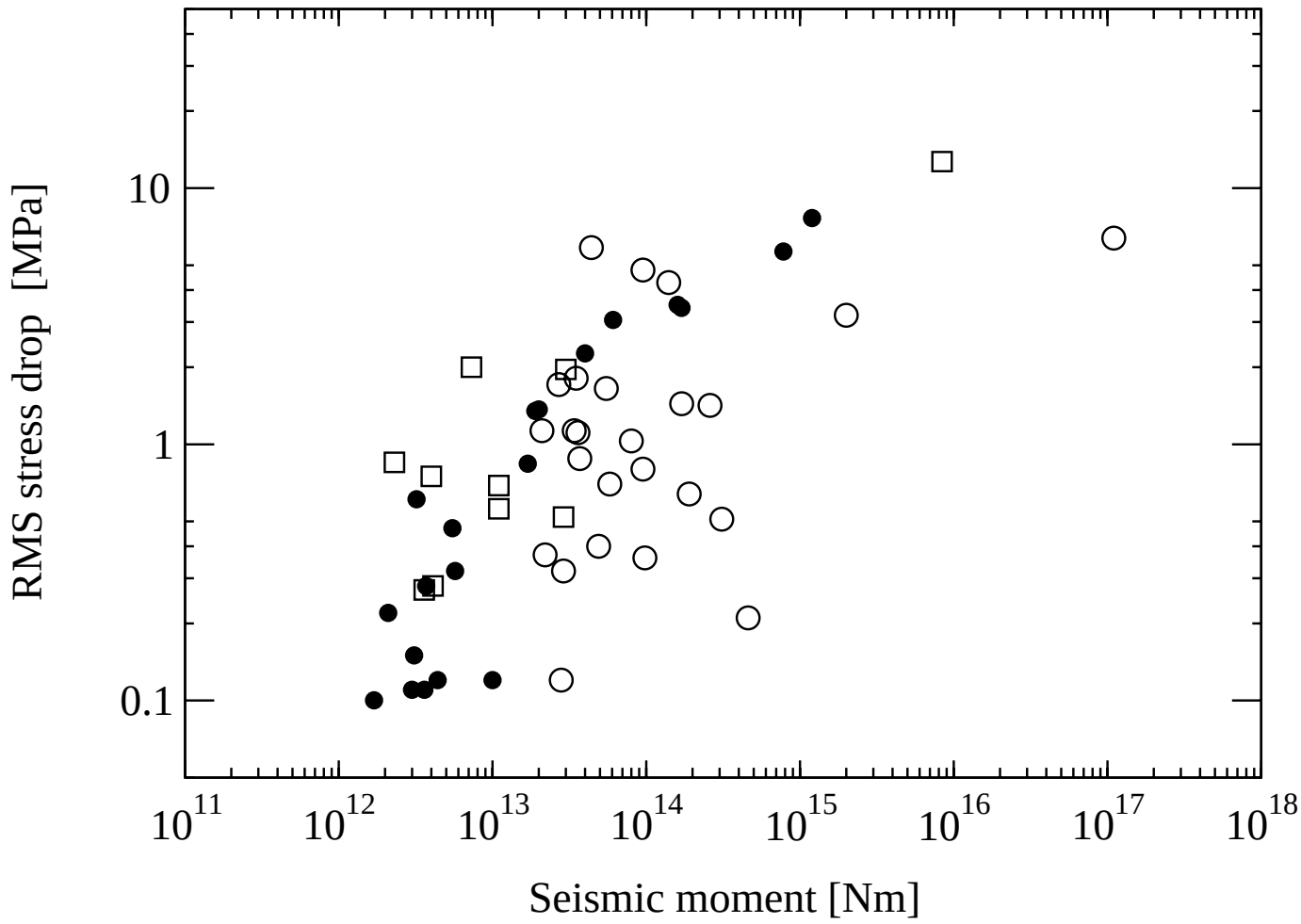
RMS stress drop [MPa]
10
1
0.1
10^{11}
10^{12}
10^{13}
10^{14}
10^{15}
10^{16}
10^{17}
10^{18}
Seismic moment [Nm]

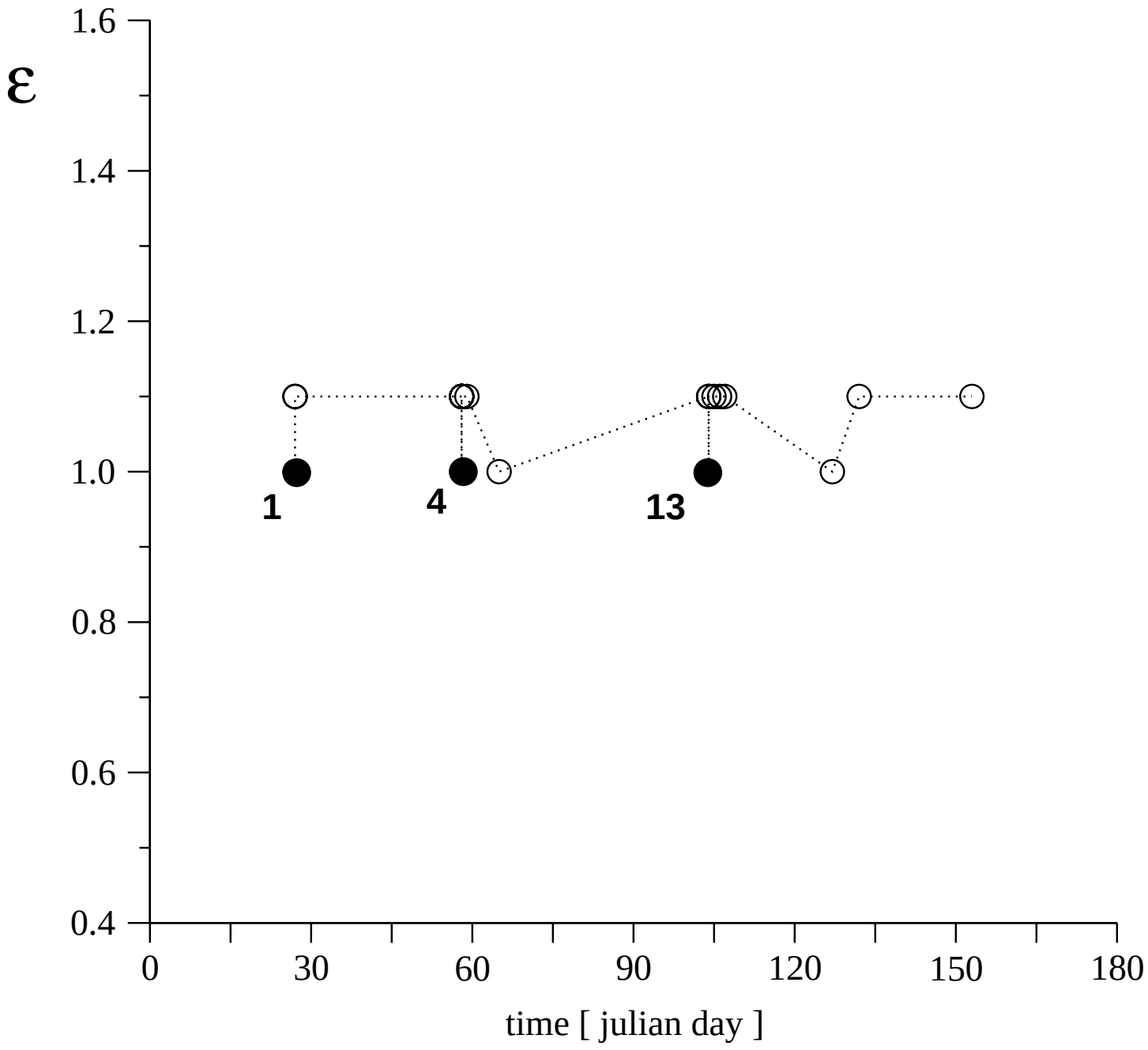
ε
1.6
1.4
1.2
1.0
0.8
0.6
0.4
0
30
60
90
120
150
180
time [julian day]
1
4
13

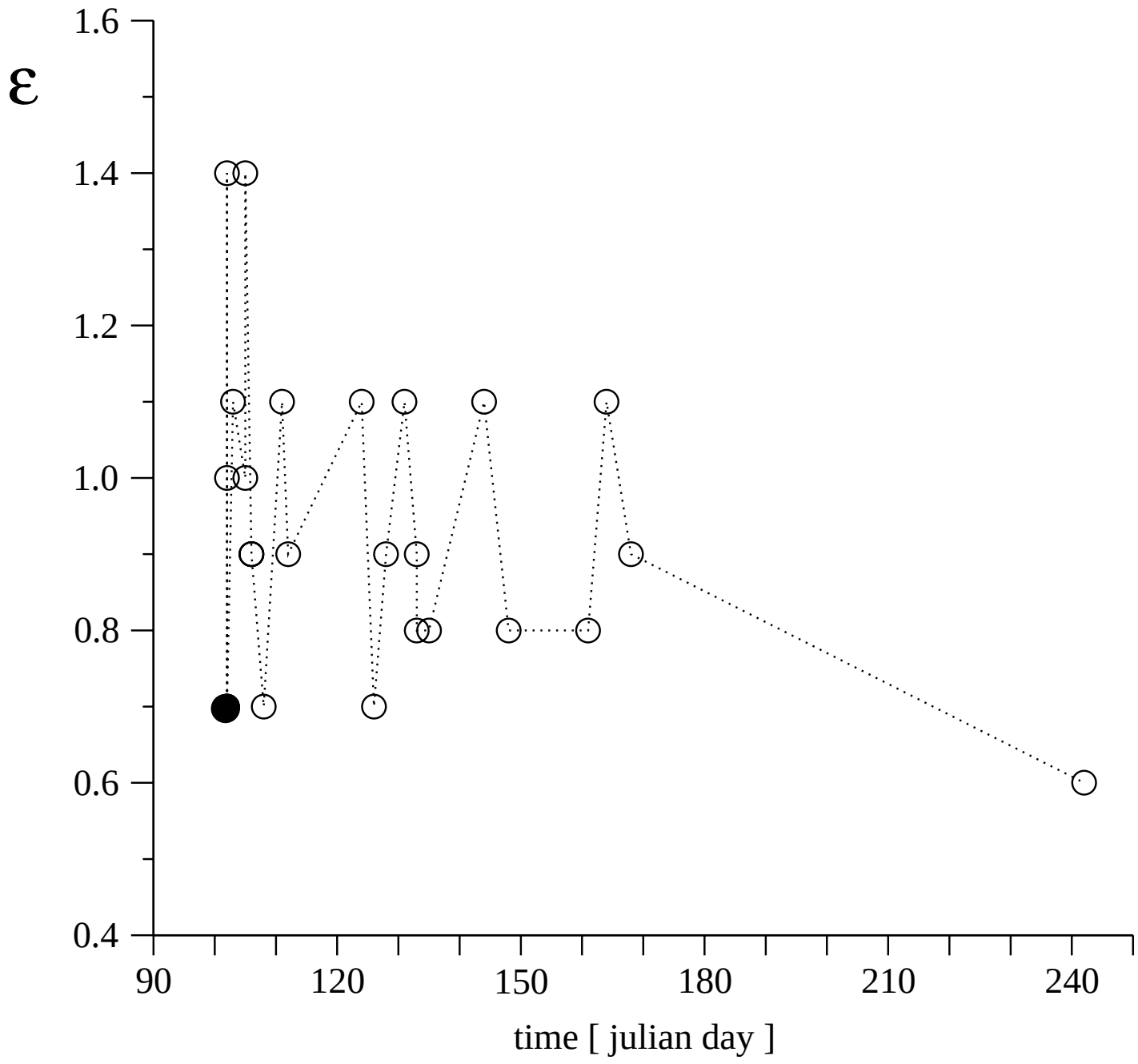
ε
1.6
1.4
1.2
1.0
0.8
0.6
0.4
90
120
150
180
210
240
time [julian day]

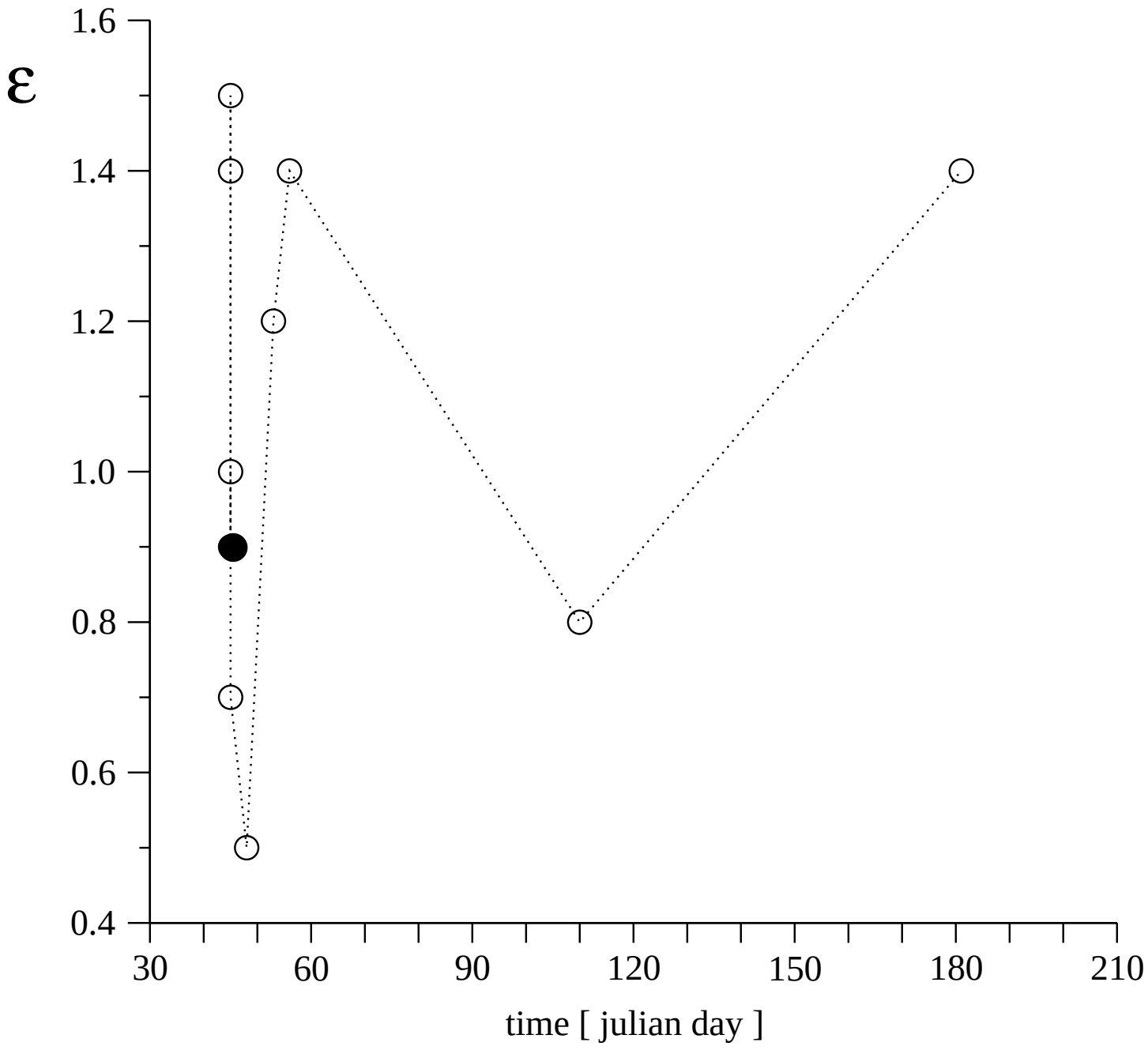
ε
1.6
1.4
1.2
1.0
0.8
0.6
0.4
30
60
90
120
150
180
210
time [julian day]

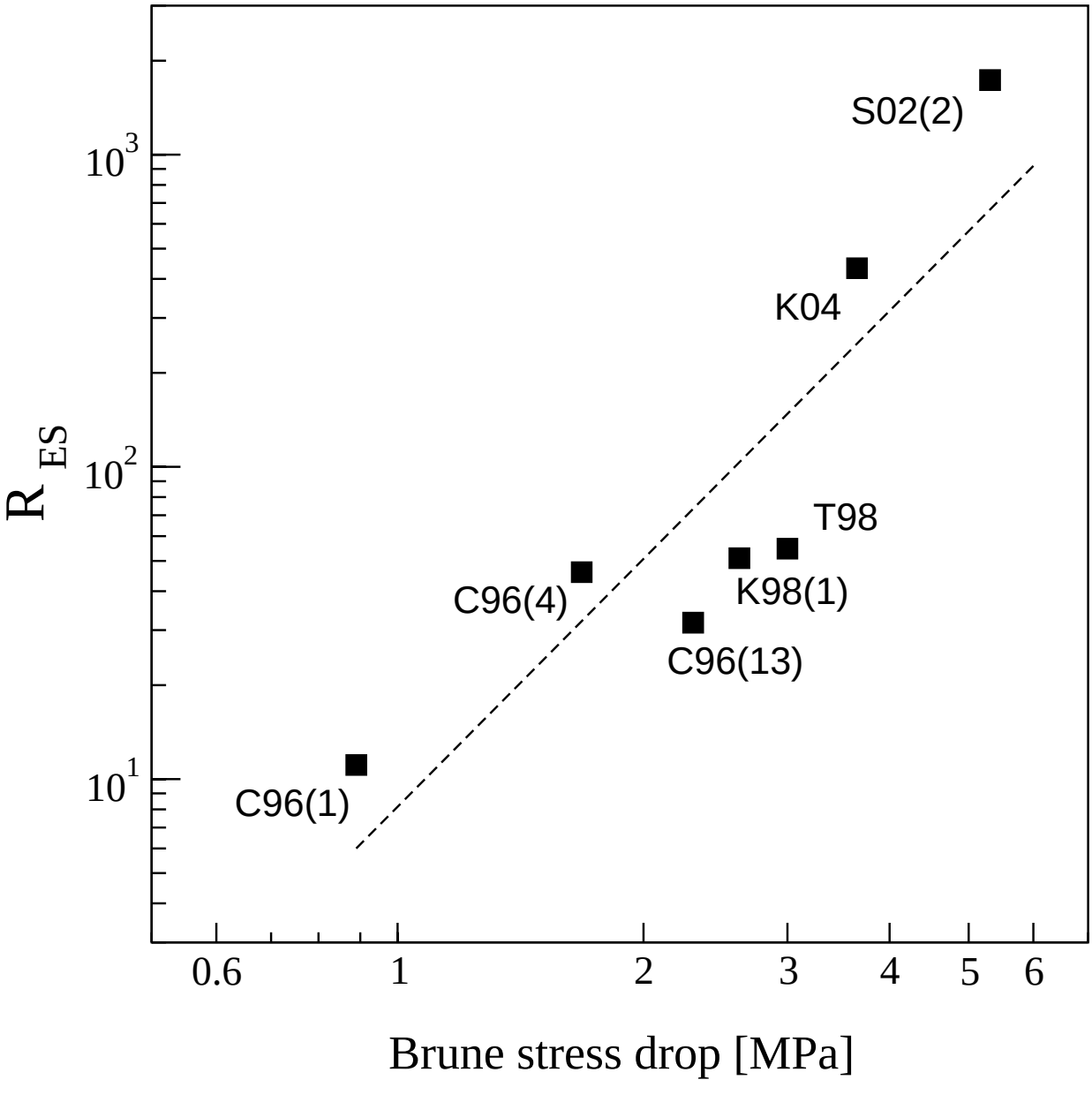
S02(2)
K04
T98
K98(1)
C96(4)
C96(13)
C96(1)
10^3
10^2
10^1
R_{ES}
0.6
1
2
3
4
5
6
Brune stress drop [MPa]